UNIV. OF MICHIGAN
JUL 14 1953

Electrochemical Society

ELECTROCHEMICAL INDUSTRY

The Golden Gulf Coast

Electrolytic Aids to

THE MODERN TEXTILE INDUSTRY

Chlorine and caustic soda, products of the electrolytic industry are essential in turning natural and man-made fibres into modern textiles of all kinds.

Uniformly high quality **GLC Graphite Anodes** are doing their share to help the electrolytic industry meet the ever increasing civilian and defense demands for chlorine and caustic soda.

ELECTRODE DIVISION

Great Lakes Carbon Corporation

Niagara Falls, N. Y. GLC Morganton, N. C.

Courtesy The Dow Chemical Company and The Saran Yarn Company

Graphite Anodes, Electrodes and Specialties

Sales office: Niagara Falls, N. Y. **Other offices:** New York N. Y., Chicago, Ill., Pittsburgh, Pa.

Sales Agents: J. B. Hayes, Birmingham, Ala., George O'Hara, Long Beach, Cal., Great Northern Carbon & Chemical Co. Ltd., Montreal, Canada

EDITORIAL STAFF

R. M. Burns, *Chairman*

Norman Hackerman, *Technical Editor*

Ruth G. Sterns, *Managing Editor*

Cecil V. King, *Associate Editor*

U. B. Thomas, *News Editor*

Mary F. Murray, *Assistant Editor*

DIVISIONAL EDITORS

J. V. Petrocelli, *Corrosion*

Abner Brenner, *Electrodeposition*

W. C. Vosburgh, *Battery*

H. C. Froelich, *Electronics*

W. C. Gardiner, *Industrial Electrolytic*

S. J. Sindeband, *Electrothermic*

John J. Chapman, *Electric Insulation*

L. B. Rogers, *Theoretical*

Sherlock Swann, Jr., *Electro-Organic*

REGIONAL EDITORS

Joseph Schulein, *Pacific Northwest*

J. C. Schumacher, *Los Angeles*

O. W. Storey, *Chicago*

C. W. Heise, *Cleveland*

Paul S. Brallier, *Niagara Falls*

Oliver Osborn, *Houston*

Earl A. Gulbransen, *Pittsburgh*

A. C. Holm, *Canada*

J. W. Cuthbertson, *Great Britain*

T. L. Rama Char, *India*

ADVERTISING OFFICE

Jack Bain

Advertising Manager

345 Fifth Avenue

New York 17, N. Y.

PHONE—*Murray Hill 2-3345*

Journal of the

Electrochemical Society

JULY, 1953 **VOL. 100 · NO. 7**

CONTENTS

Editorial

Consumer Contribution to Chemical Industry 171*C*

Regional Feature

The Golden Gulf Coast 173*C*–187*C*
Five articles by *Oliver Osborn, F. L. Kaestle, W. J. Rave, Frank Chrencik, and H. Lee Norris, Jr.*

Technical Papers

Structural Properties of Some Synthetically Prepared Manganese Dioxides. *G. Butler and H. R. Thirsk* 297
Oxidation of Metals at High Temperatures. *Walter J. Moore.* 302
Surface Reactions of Steel in Dilute $Cr^{51}O_4^{=}$ Solutions: Applications to Passivity. *R. A. Powers and Norman Hackerman* 314
Quinones as Ion Source in Hydrocarbons. *Andrew Gemant* .. 320
Formation of Immersion Zinc Coatings on Aluminum. *W. G. Zelley* 328
Polarography of Thioglycolic Acid. *D. L. Leussing and I. M. Kolthoff* 334

Feature Section

The Mechanism of Electropolishing of Copper in Phosphoric Acid Solutions, I. Processes Preceding the Establishment of Polishing Conditions. *J. Edwards* 189*C*

Current Affairs

Wrightsville Beach Offers Many Attractions for Fall Meeting. 195*C*
Seventh Annual Battery Research and Development Conference 196*C*
Highlights of the Board of Directors' Meeting 197*C*
News Notes ..... 198*C* Personals 200*C*
Division News ..... 198*C* New Members 201*C*
Section News ..... 199*C* New Products 202*C*
Annual Report of the Board of Directors and Secretary 203*C*
Treasurer's Report 204*C*

Published monthly by The Electrochemical Society, Inc., Mount Royal and Guilford Aves., Baltimore 2, Md., combining the JOURNAL and TRANSACTIONS OF THE ELECTROCHEMICAL SOCIETY. Editorial offices: 216 West 102nd Street, New York 25, N. Y. Statements and opinions given in articles and papers in the JOURNAL OF THE ELECTROCHEMICAL SOCIETY are those of the contributors, and The Electrochemical Society assumes no responsibility for them. Subscription $11.25 to members, $15.00 to nonmembers. Single copies $1.25 to members, $1.50 to nonmembers. Copyright 1953 by The Electrochemical Society, Inc. Entered as second-class matter November 15, 1947, at the Post Office at Baltimore, Md., under the act of August 24, 1912

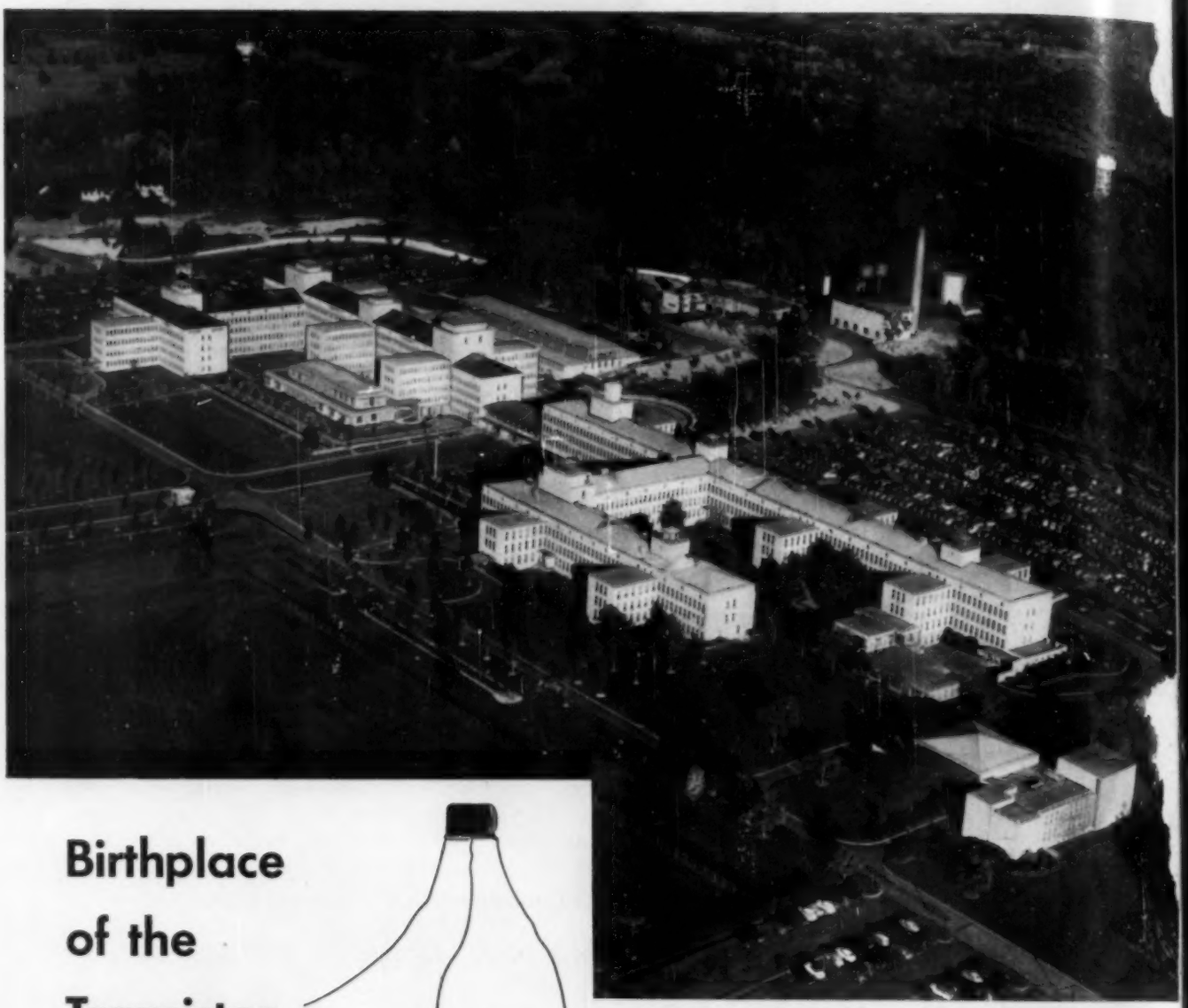

Birthplace of the Transistor

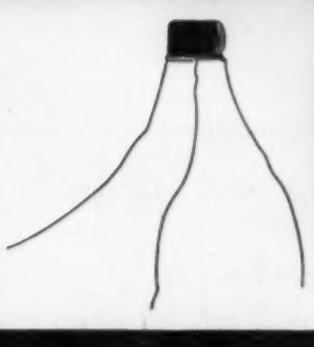

Bell Telephone Laboratories at Murray Hill, N. J. Other laboratories are in New York City and at Whippany and Holmdel, N. J.

The ***Transistor,*** that revolutionary new electronics device, is a product of *telephone* research. It was conceived, invented and developed at Bell Telephone Laboratories by men in search of ways to improve telephone service. It was announced just five years ago.

The ***Transistor*** can do most of the things that vacuum tubes can do—and others, too—but it is not a vacuum tube. It works on entirely new physical principles. Rugged, simple and tiny, the Transistor uses incredibly small amounts of power—and then only when actually operating.

Transistors promise smaller and cheaper electronic equipment and the spread of electronics where other equipment has not been able to do the job as economically. They are already at work in the Bell System, generating the signals that carry dialed numbers between cities, and selecting the best route for calls through complex switching systems. Engineers see many other possibilities: for example, as voice amplifiers in telephone sets to aid the hard of hearing, and as switches.

Recognizing the tremendous possibilities of the ***Transistor*** in every phase of the electronics industry, the Bell System has made the invention available to 40 other companies. Thus, again, basic research to improve telephony contributes importantly to many other fields of technology as well.

TRANSISTOR SUMMARY

Basically, a ***Transistor*** is a tiny wafer of germanium with three electrodes, over-all about the size of a coffee bean.

It can amplify signals 100,000 times on much less power than a pocket flashlight requires. This opens the door to its use in smaller telephone exchanges where vacuum tube equipment would be too costly to operate.

Unlike a vacuum tube, the ***Transistor*** has no vacuum and no filament to keep hot. It operates instantly, without "warm-up" delay. The Transistor can also be used as an electric eye and to count electrical pulses.

BELL TELEPHONE LABORATORIES

Improving telephone service for America provides careers for creative men in scientific and technical fields.

Structural Properties of Some Synthetically Prepared Manganese Dioxides[1]

G. Butler and H. R. Thirsk

Laboratories of Physical Chemistry and Coke Research, King's College, Newcastle upon Tyne, England

ABSTRACT

Various forms of manganese dioxide have been made by methods described in the literature and examined by chemical analysis, x-ray and electron diffraction, and electron microscopy. Conclusions reached by previous workers mainly from x-ray analysis have, in general, been confirmed, but some new facts emerge, the most important being evidence of slightly differing forms of α-MnO_2 dependent in part on crystal size, and of the presence of layers of MnO and γ-Mn_2O_3 or Mn_3O_4 on the surface of certain of the preparations.

Introduction

Elucidation of the structure of naturally occurring manganese dioxides has proved to be a topic of very great difficulty. Owing to the importance of this material in electrochemical applications, a good deal of attention has recently been paid to the nature of materials prepared synthetically under controlled conditions. Out of many references to work of this nature we quote three of a general character; a paper on the solid oxides and hydroxides of manganese by Moore, Ellis, and Selwood (1), a review of certain better characterized manganese oxides by Cole, Wadsley, and Walkley (2), and a study of manganese dioxides by Delano (3) based on several thousand x-ray diffraction photographs.

From a consideration of these and other papers, the following general conclusions on the state of knowledge of the manganese oxides may be made. Three forms of manganese dioxide exist, α-MnO_2 or cryptomelane, β-MnO_2 or pyrolusite, and γ-MnO_2 or ramsdellite. The designation γ has also been used for certain dispersed forms of manganese dioxide, but since opinion seems to be in favor of these being poorly crystalline ramsdellite no confusion exists in giving this name to both. A further modification, manganous manganite, is known which changes to α-MnO_2 on heating. Of the lower oxides, two varieties of Mn_2O_3 are known to exist, α and γ, the x-ray diffraction pattern from the form being almost identical to that given by Mn_3O_4. The monoxide, MnO, completes the series.

Recently we have had occasion to prepare a large number of samples of manganese dioxide for electrochemical examination and this has given us an opportunity of carrying out chemical analyses and structural examinations, the latter by electron microscopy, and x-ray and electron diffraction. Some interesting points have emerged from this study and are described below.

[1]Manuscript received March 5, 1952. This paper was prepared for delivery before the Montreal Meeting, October 26 to 30, 1952.

Experimental

X-Ray, Electron Microscope, and Electron Diffraction Techniques

Photographs of the manganese oxides, prepared as rod-shaped specimens about 0.3 mm in diameter with water and gum tragacanth, were taken on a Metropolitan-Vickers demountable x-ray set using a 9 cm powder camera. Unfiltered iron radiation was used, the manganese dioxide specimen acting as its own β filter. The wave length of the α radiation was taken to be 1.9373 Å (4).

The electron micrographs were obtained, using standard techniques, by means of a Metropolitan-Vickers E.M.3 instrument, and most of the electron diffraction was also carried out on the same instrument. This enabled a direct comparison to be made between the appearance of the specimen and a diffraction pattern from a related portion of the observed image. Some use was also made of an electron diffraction instrument of the type described by Finch (5).

For an accurate determination of the interplanar spacings by electron diffraction we used thallous chloride as a codeposited standard, as suggested recently by Boswell (6). $a_o = 3.834$ Å was taken as the length of the edge of the cubic cell (7).

Preparative and Analytical Techniques

All materials used were of Analar purity and solutions were made up with distilled water.

The samples obtained were analyzed for available oxygen, that is oxygen in excess of the formula MnO, total water, and, in some cases, potassium. Available oxygen was determined by the method of Eberius and Le Blanc (8) in which the oxide is

TABLE I. *Preparative methods and analytical data*

Preparative method	Comments on preparation	Analysis
1. β-MnO_2 from manganese nitrate	Modified Bhatnagar procedure [see (1) p. 863]	$MnO_{1.98}\cdot 0.2H_2O$
2. $MnSO_4$ + $(NH_4)_2S_2O_8$	[See (10) p. 3040 and (1) p. 865]. Washed by decantation with hot water and filtered through a No. 4 sintered glass filter 2*a*. Dried over concentrated H_2SO_4 for several days, and finally over phosphoric acid 2*b*. Dried at 60°C for several days 2*c*. Dried at 100° C for several days	2*c*. $MnO_{1.95}\cdot 0.25$ H_2O agreeing exactly with Selwood, *et al.*, (10). No potassium found but there seemed to be some ammonia present which was not removed by heating for 24 hr at 200°C in oxygen
3. $K\cdot MnO_4$ + $MnSO_4$ + KNO_3	Same as for the method given in (1) p. 3040, for the preparation of the γ II oxide except the preparation was separated through a No. 4 sintered glass filter. The sulfate-nitrate solutions were divided into portions (*a*), (*b*) and (*c*) and treated separately, in the case of (*c*) with a considerable excess of permanganate. These preparations were dried at 100°C	Not so reproducible as for 2, e.g., 3*a*. $MnO_{1.93}\cdot 0.17$ H_2O 3*b*. $MnO_{1.90}\cdot 0.20$ H_2O 3*c*. $MnO_{1.88}\cdot 0.41$ H_2O
4. 100 g $KMnO_4$ in 600 ml distilled water. 50 ml concentrated HCl added drop wise	Washed by decantation and finally separated through a No. 4 sintered glass filter 4*a*. Dried at 100°C 4*b*. Used directly for diffraction and microscopy	(*a*) Analyzed as $MnO_2\cdot 0.82$ H_2O and (*b*) as $MnO_{1.928}$ but both were associated in addition with $(K_2O)_{0.139}$
5. Commercial B.D.H. sample of manganese	Some of this sample was heated at 530°C for 100 hr	Composition as received $(K_2O)_{0.106}$ $MnO_{1.92}$ $(H_2O)_{1.69}$

TABLE II. *Structural details*

	Results from x-ray and electron diffraction and electron microscopy
Prep. 1.	Well crystallized. Indexed on a b.c. tetragonal unit cell with $a_o = 4.404 \pm 0.001$ Å; $c_o = 2.873 \pm 0.001$ Å. E.D.: superimposed patterns from relatively few single crystals of β-MnO_2. Electron microscopy showed massive aggregates of relatively small surface area.
Prep. 2.	Very diffuse x-ray diffraction lines with spacings 4.03, 2.42, 2.12, 1.63, 1.39, 1.06 Å agreeing almost exactly with Selwood, *et al.* (1). Electron micrograph of 2*a*, *b*, and *c* showed remarkable agglomerates and straw shaped particles as shown in Fig. 1 and 2. Fig. 2 closely resembles an electron micrograph taken from α-MnO_2 by McMurdie and Golavato (11). Electron diffraction showed three different patterns either singly or together corresponding to: (*a*) A face-centered cubic structure, Fig. 3, identified as MnO (rock salt structure) $a_o = 4.43$ Å (*b*) Sharp diffractions of either Mn_3O_4 or γ-Mn_2O_3 as described in (1). (*c*) A highly resolved pattern of a type described by Butler and Thirsk (12) from α-MnO_2 with a body-centered tetragonal unit cell calculated as: $a_o = 9.88 \pm 0.03$ Å, $c_o = 2.845 \pm 0.005$ Å, $a_o/c_o = 3.47$. The c_o axes of small crystallites in parallel array lying along the long axis of the needles of Fig. 2 which thus are composite.
Prep. 3.	X-ray analysis for these comparable preparations showed them to be very different in structure. All the lines were rather diffuse. 3*a*. Mixture of the γ form with some α-MnO_2. 3*b*. α-MnO_2 predominated over the γ form. 3*c*. Only α-MnO_2 observed. Electron micrographs similar to Fig. 2; aggregates similar to Fig. 1 not observed. Electron diffraction gave the three patterns as described above but the α-MnO_2 was more finely crystalline. In this case the pattern corresponded to a body-centered tetragonal lattice with $a_o = 9.81 \pm 0.003$ Å, $c_o = 2.86 \pm 0.01$ Å, $a_o/c_o = 3.43$. By x-rays the dimensions for the α-MnO_2 were $a_o = 9.85 \pm 0.02$ Å; $c_o = 2.852 \pm 0.006$ Å; $a_o/c_o = 3.45$.
Prep. 4 and 5.	X-ray photographs of preparations 4 and 5 were identical and corresponded to manganous manganite. The *d* spacings for preparation 4 are listed in Table III together with those for the corresponding oxide prepared by Copeland, Griffith and Schertzinger (13). They are to be compared in the same table with the two preparations of α-MnO_2 referred to above and with the pattern from preparation 5 after sintering, showing this preparation after heat-treatment also to have become a well crystallized α-MnO_2.

heated with hydrochloric acid, the chlorine evolved being forwarded by carbon dioxide and adsorbed in potassium iodide solution. The iodine liberated estimated by titration with a sodium thiosulfate solution, standardized against potassium iodate.

Water was estimated by Penfield's method (9) and potassium by a flame photometer.

The various oxides were prepared as shown in Table I, most of the methods being quite standard. Table II includes x-ray and electron diffraction data and comments on the electron microscopy. Table III

seem to do justice to the analyses. He determined available oxygen, total manganese, and water. From each of the first two, the percentage manganese dioxide was calculated and the composition given as a mean of the two different determinations. We prefer to express the manganese in terms of manga-

TABLE III. *Comparison of the reflections of manganous manganite and* α-MnO_2

Prep. 4a		Prep. 5		Manganous manganite prepared by Copeland, Griffiths, and Schertzinger (13)		Prep. 3c		Prep. 5 heated at 530°C for 100 hr		
I	d	I	d	I	d	I	d	I	d	hkl
S	7.39	S	7.25	MS	7.13	S	7.03	S	7.00	110
						M	4.94	S	7.92	200
VW	3.64	VW	3.63	W	3.53	VW d	3.49	W	3.48	220
						MS vd	3.12	VS	3.12	130
								VW	2.452	400
W	2.43	W	2.44	M	2.41	S vd	2.401	S	2.396	121
								VW	2.195	240
				VW d	2.14	M d	2.150	S	2.151	301
								VW	1.926	150
						W d	1.826	MS	1.832	141
								VW d	1.637	600
						W d	1.539	MS	1.540	251
W	1.415	W	1.414	VW	1.418	W	1.424	M	1.430	002
						VW d	1.355	M d	1.354	451
								VW	1.298	312
a_o = 10.4		a_o = 10.3		a_o = 10.0		a_o = 9.85 ± 0.02		a_o = 9.83 ± 0.01		
c_o = 2.84		c_o = 2.84		c_o = 2.84		c_o = 2.852 ± 0.006		c_o = 2.862 ± 0.003		
a/c = 3.65		a/c = 3.63		a/c = 3.52		a/c = 3.454		a/c = 3.434		

All reflections from preparation 4a and preparation 5 as received were diffuse, from preparation 5 sintered, sharp. VS, very strong; S, strong; MS, medium strong; M, medium; W, weak; VW, very weak; d, diffuse; vd, very diffuse. All cell dimensions in A.

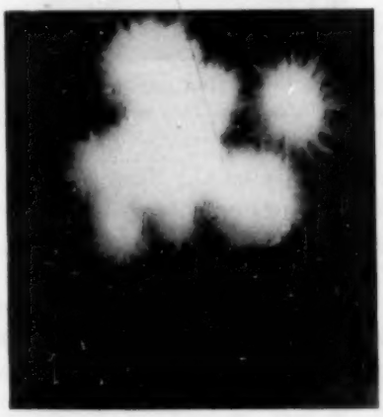

FIG. 1. Electron micrograph of MnO_2 prepared from ammonium persulfate and manganous sulfate. Gold shadowed 45°. × 5300.

is concerned particularly with the effect of sintering on the oxides.

DISCUSSION

Table I is self-explanatory except in the case of preparation 2. Glemser (14) gives the formula of the oxide prepared in this way as $MnO_{1.93}$. Glemser's results, however, require further examination since his figures for the oxygen/manganese ratio do not

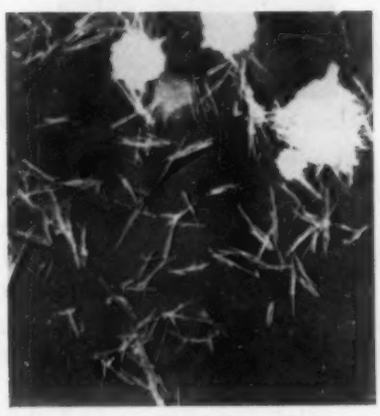

FIG. 2. Electron micrograph of α-MnO_2 formed in preparation 2. Gold shadowed 45°. × 5300.

nese oxide. A general formula for a manganese oxide may then be written as $xMnO \cdot yO^* \; zH_2O$ (where O^* is the available oxygen) which may be rearranged as $MnO_{1+y/x} \cdot \frac{z}{x} H_2O$. When Glemser's results are recalculated in this way, the values for the oxygen/manganese atomic ratio are in better agreement with the values of other workers. In the present case, the formula of Glemser's oxide becomes $MnO_{1.96} \cdot 0.30\ H_2O$. It appears, therefore, that this

method of preparation gives an oxide of reproducible composition.

The electron micrographs given by preparation 4 resembled those of Fig. 1, but the oxide was apparently in a more finely dispersed state. This was confirmed by the electron diffraction patterns. The latter only showed MnO with certainty and more diffuse patterns which corresponded with the presence of Mn_3O_4 or γ-Mn_2O_3.

The electron diffraction patterns from preparation 5 before heat-treatment corresponded to those previously described as due to MnO and Mn_3O_4. No other characteristic pattern was observed.

Attempts were made to remove the surface oxide layers from these preparations by prolonged refluxing with nitric acid followed by washing and drying at room temperature, but we were unable to make any alteration detectable by electron diffraction; the conclusion is reached that, in the cases described, definite lower oxides of manganese are present on the surfaces of the aggregates and fine

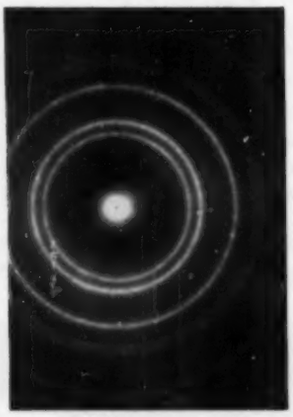

FIG. 3. Electron diffraction picture from surface oxide (MnO).

particles may consist almost entirely of the lower oxides. In view of the very large surface of some of the specimens, the presence of lower oxides must contribute significantly to the departure from stoichiometry of the mass of material if, as is customary, one regards the dioxide as a homogeneous material.

A criticism of this work may be levelled at the possibilities of decomposition taking place during the photographing of the specimens by the combined action of the electron beam and the high vacuum.

It was suggested to the authors[2] that there might be some possibility of reduction by traces of vacuum oil in the system. The phenomena of carbon deposition on specimens by the action of the electron beam is well known and may be demonstrated very clearly by glancing incidence electron microscopy. There is little doubt that the process must occur during the examination of our oxides, although no evidence was found of the characteristic pattern from cracked carbon films.

Glemser and Einerhand (15), studying the higher nickel oxides, reported the presence of nickelous oxide by electron diffraction, but associated in this case with apparent decomposition of the specimen.

We have noted the presence of NiO in higher nickel oxides when using electron diffraction, but unfortunately our specimens are of such a form that electron microscopy is incapable of showing any change in the appearance of the specimen. It should be added that the Finch instrument with silicone-filled diffusion pumps yields results with both the manganese and nickel oxides similar to those with the E.M.3 instrument.

Some of the above experimental observations would indicate that reduction in the beam is quite a possibility. Nevertheless the authors do not consider them to be conclusive. The lower oxides are not observed in all the specimens and when they are

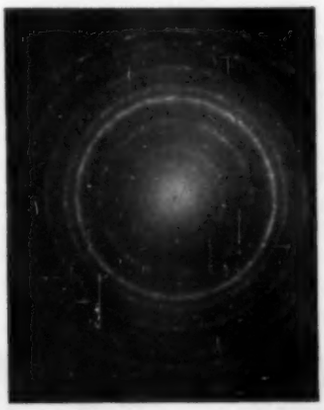

FIG. 4. Electron diffraction pattern from α-MnO_2 prepared from ammonium persulfate and manganous sulfate.

seen, not necessarily on the most reactive dioxides; preparation 5, for example, was very unreactive but shows strong MnO diffractions.

The whole phenomenon seems to be one requiring the most careful examination, particularly from workers dealing with reducible systems and using electron diffraction and microscopy. The point is of importance since electron diffraction is by far the most powerful technique for surface studies of this type and a knowledge of these effects, whether artifacts or not, is most essential.

Several interesting points emerge from an examination of the data in Table III. First, the process of increasing crystallinity is accompanied by a large decrease in the a_o parameter, the c_o parameter changing but slightly. This is best shown by the variation in a_o/c_o. This would infer that the Copeland, Griffiths, and Schertzinger preparation is more highly crystalline than either of our own, a fact which is borne out by the appearance of an extra

[2] By private communication from N. C. Cahoon.

reflection (301) in the diffraction photograph from their oxide. Second, preparation 3*c*, which from the diffuseness of the diffraction lines is not as crystalline as the heated preparation 5, is shown to have a slightly larger unit cell. What the actual rearrangement within the unit cell corresponding to these changes in cell dimensions is we can only surmise, but this may be solved by closer attention to and measurement of the actual intensities during recrystallization. Here we seem to have good evidence that manganous manganite is a poorly crystalline form of α-MnO_2.

Acknowledgments

The authors would like to thank Professor W. F. K. Wynne-Jones for the excellent facilities placed at their disposal and for the interest he has shown in the work. They would also like to thank Mr. E. H. Boult for experimental assistance with the electron microscopy.

Any discussion of this paper will appear in a Discussion Section, to be published in the June 1954 issue of the Journal.

References

1. T. E. Moore, M. Ellis, and P. W. Selwood, *J. Am. Chem. Soc.*, **72**, 856 (1950).
2. W. F. Cole, A. D. Wadsley, and A. Walkley, *Trans. Electrochem. Soc.*, **92**, 133 (1947).
3. P. H. Delano, *Ind. Eng. Chem.*, **42**, 523 (1950).
4. W. L. Bragg, *J. Sci. Instr.*, **24**, 27 (1947).
5. G. I. Finch and H. Wilman, *Ergeb. exakt. Naturw.*, **16**, 353 (1937).
6. F. W. C. Boswell, *Proc. Phys. Soc. London, A*, **64**, 465 (1951).
7. R. W. C. Wyckoff, "Crystal Structures," Interscience Publishers Inc., New York (1948).
8. E. Eberius and M. Le Blanc, *Z. physik. Chem.*, **160A**, 129 (1932).
9. S. L. Penfield, *Am. J. Sci.*, **48**, 30 (1894).
10. P. W. Selwood, H. P. Eischens, M. Ellis, and K. Wethington, *J. Am. Chem. Soc.*, **71**, 3039 (1949).
11. H. F. McMurdie and E. Golovato, *J. Research Natl. Bur. Standards*, **41**, 589 (1948).
12. G. Butler and H. R. Thirsk, *Acta Cryst.*, **5**, 288 (1952).
13. L. C. Copeland, F. S. Griffiths, and C. B. Scherzinger, *Trans. Electrochem. Soc.*, **92**, 127 (1947).
14. O. Glemser, *Ber.*, **72**, 1879 (1939).
15. O. Glemser and J. Einerhand, *Z. anorg. Chem.*, **261**, 431 (1950).

Oxidation of Metals at High Temperatures[1]

WALTER J. MOORE

Department of Chemistry, Indiana University, Bloomington, Indiana

ABSTRACT

The available data on the oxidation rates of pure metals from 300° to 1000°C have been analyzed in terms of concentrations of defects in the oxide structures and defect diffusion coefficients. Quantitative agreement with the diffusion theory is obtained in the cases of *p*-type oxides such as cuprous oxide and nickel oxide, in which cationic vacancies arise by solution of oxygen at the oxide-oxygen interface. The parabolic oxidation rates in the cases of some *n*-type oxides, such as zinc oxide and zirconium oxide, are characterized by low activation heats and large negative activation entropies. In some of these cases anionic diffusion seems likely. In the case of zinc oxide, the diffusion of radiozinc during oxidation supports the cationic diffusion mechanism. The data on linear oxidation rates fall into two classes; evidence is presented to show that one class represents reaction at the oxide-oxygen interface, and the other, reaction at a metal-oxygen interface.

INTRODUCTION

Considerable new data have been obtained in recent years on the oxidation rates of pure metals from 300° to 1000°C. It is the purpose of this paper to analyze the factors that control the absolute values of these rates. Our understanding of these reactions is based on the pioneer experimental and theoretical work of Wagner (1) and on the Wagner-Schottky analysis of defects in ionic crystals (2).

The present treatment is divided into six sections: (*a*) the empirically observed rate laws are set forth; (*b*) the laws of diffusion of reactants through a growing oxide film are described; (*c*) the defects in oxide structures, which provide diffusion mechanisms, are discussed in terms of statistical thermodynamics; (*d*) cationic diffusion coefficients in metal oxides are analyzed in terms of defect concentration and defect mobility; (*e* and *f*) the observed oxidation rate constants are related to the results of the preceding sections.

EMPIRICAL RATE LAWS

If a coherent, nonscaling oxide film is formed, most of the measurements of metal oxidation above 300°C can be fitted to the *parabolic law*,

$$dy/dt = k_1/y \qquad \text{(I)}$$

where k_1 is the *parabolic rate constant*. On integration with the initial conditions, $y = y_0$ at $t = 0$, equation (I) becomes

$$y - y_0 = \Delta y = 2k_1(t/\Delta y) - 2y_0 . \qquad \text{(II)}$$

This is probably the best form in which to apply the law, since it allows one to discard the initial oxygen uptake, and to set the origin of time, $t = 0$, at any desired film thickness y_0. If the law is followed, a plot of y against $(t/\Delta y)$ gives a straight line, the slope of which is $2k_1$, and the intercept, $-2y_0$. The calculated y_0, however, will usually have little quantitative significance, in view of the uncertain initial surface area, nonisothermal initial conditions, and possible departures from the parabolic growth law in the first stages of oxidation. The advantage of the use of equation (II) is that it provides a method for discarding all these initial uncertainties.

In some cases a linear growth law has been observed, $dy/dt = k_0$. The transition from a parabolic to a linear rate is usually associated with a breakdown of the film, as, for example, in the oxidation of magnesium above 500°C (3). In some cases, however, a linear law has been observed even with a coherent film, for example, in the oxidation of titanium above 800°C (4), or in the oxidation of molybdenum with nitric oxide (5). In such instances, it has been concluded that the diffusion of reactants through the film is rapid compared to the actual interface reaction rate.

An intermediate type of rate law has also been considered,

$$dy/dt = k_1/(k_2 + y). \qquad \text{(III)}$$

This represents a case in which diffusion and interface reactions have comparable specific rates. On integration with $y = 0$ at $t = 0$, equation (III) yields

$$y = 2k_1(t/y) - 2k_2 . \qquad \text{(IV)}$$

This expression is identical in form with equation (II), and in no experiments so far reported have the effects of an initial surface film and of a possible

[1] Manuscript received March 24, 1952. This paper was prepared for delivery before the Montreal Meeting, October 26 to 30, 1952.

departure from the parabolic law been adequately separated. Instead of trying to make this separation by an analysis of initial rates, it would appear to be more useful to study systems to which equation (III) might apply even over extended periods of reaction. Such systems might be expected at high temperatures and low oxygen pressures when the oxide film is an oxidation semiconductor like cuprous oxide. For example, it has been reported (6) that the oxidation of pure iron in carbon dioxide-carbon monoxide mixtures follows a parabolic law below 900°C and a linear law at 1000°C, so that the intermediate region might provide a suitable experimental illustration of equation (IV).

The Diffusion Problem

The typical situation that arises during the growth of an oxide film on a metal is shown in Fig. 1. To focus attention on a concrete example, let us suppose that the metal ions diffuse through the oxide, by way of interstitial positions, and react at the oxide-oxygen interface. The diffusion of oxygen in the opposite direction is assumed to be negligible. If the concentration of interstitial ions at any point x in the oxide is c_i, and the diffusion coefficient for the interstitial ions is D_i, the diffusion is governed by the equation

$$D_i \delta^2 c_i/\delta x^2 = \delta c_i/\delta t. \qquad \text{(V)}$$

The problem is complicated by the motion of the outer boundary, at $x = y(t)$. If we introduce $r = x/y$, equation (V) becomes

$$D_i y^{-2} \delta^2 c_i/\delta r^2 = \delta c_i/\delta t - r y^{-1} y' \delta c_i/\delta r \qquad \text{(VI)}$$

where $y' = dy/dt$. It is evident that the equation is separable only if $yy' = k_1$, i.e., the parabolic rate law. In this case,

$$(D_i/k_1)\delta^2 c_i/\delta r^2 + r\delta c_i/\delta r = 2t\delta c_i/\delta t. \qquad \text{(VII)}$$

With the boundary conditions $c_i = c_0$ at $r = 0$; and $c_i = c_1$ at $r = 1$, the solution of equation (VII) is

$$c = c_0 + \frac{c_1 - c_0}{\text{erf } (k_1/2D_i)^{\frac{1}{2}}} \text{erf } [(k_1/2D_i)^{\frac{1}{2}} r]. \qquad \text{(VIII)}$$

This represents a steady-state solution of the diffusion equation, so that $c = c(r)$ for all t, but c is not a linear function of r, as c would be of x in the case of a stationary outer boundary.

The growth rate of the film is

$$dy/dt = k_1/y = -D_i(\delta c_i/\delta x)_{x=y}(n_i + c_1)^{-1} \qquad \text{(IX)}$$

where n_i is the number of metal ions per unit volume in a stoichiometric oxide structure. Hence,

$$k_1 = -D_i(n_i + c_1)^{-1}(\delta c_i/\delta r)_{r=1}. \qquad \text{(X)}$$

Writing $(k_1/2D_i)^{1/2} = z$, we obtain the solution as given by Booth (7),

$$\pi^{1/2} z \exp(z^2) \text{ erf}(z) = (c_0 - c_1)(n_i + c_1)^{-1}. \qquad \text{(XI)}$$

The relation between k_1 and the diffusion coefficient D_i is obtained by solving this equation. A simple result is found when $z << 1$, i.e., when $(k_1/2D_i)$ is a small fraction. It will be shown in equation (XII) that $k_1/D_i \sim f_i$, the fraction of defects in the oxide, interstitial ions in this example. Since f_i is usually below 10^{-3}, it is possible to apply the solution of equation (XI) valid for small z to most practical cases. Since c_1 is much less than n_i, equation (XI) thus becomes

$$2z^2 = (c_0 - c_1)\, n_i^{-1} = f_0 - f_1 \qquad \text{(XII)}$$

and

$$k_1 = D_i (f_0 - f_1).$$

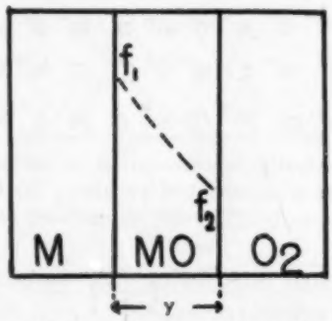

Fig. 1. A growing oxide film on a metal. The mole fractions of interstitial metal ions at the interfaces are f_1 and f_2.

This is exactly the expression obtained for steady diffusion through a slab of constant thickness.

The general solution of equation (VII) is

$$c = \exp(z^2 r^2/2) \sum_A t^{-A/2} \cdot [\alpha_A F_{1+A}(\sqrt{2}zr) + \beta_A F_{1+A}(\sqrt{2}izr)]. \qquad \text{(XIII)}$$

The $F(\sqrt{2}zr)$ are the parabolic cylinder functions. It is necessary to consider whether any solutions of this form can be found for physically reasonable boundary conditions. The requirement that the film growth proceeds through the diffusion of metal imposes in itself a boundary condition, operative at $r = 1$,

$$(-D_i/y)\ (\delta c_i/\delta r)_{r=1} = (n_i + c_i)_{r=1}^{-1}(dy/dt).$$

If we try to fit this condition with conditions representing reaction rate expressions at either boundary, we are led back to the time-independent solution with constant concentrations at each boundary as the only possible answer. Thus a necessary condition for the parabolic growth law of an oxide film, if the growth rate is controlled by diffusion, is that the

concentrations of the diffusing species be constant at the boundaries.

The problem of the growth law with a rate-determining reaction at the outer boundary has not yet been solved for the case of a moving boundary. By analogy with the above discussion, however, it may be expected that the corresponding solution for a stationary boundary is a good approximation if the defect concentration in the oxide is small. Let us consider, therefore, a layer of oxide extending from $x = 0$ to $x = y$, with a constant concentration of interstitial ions at the metal-oxide interface, and a first-order surface reaction with rate constant k_2 cm sec^{-1} at the oxide-oxygen interface. By analogy with the solution of the exactly corresponding

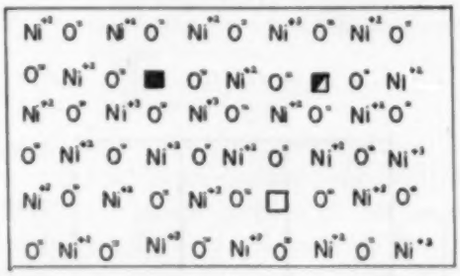

FIG. 2. Schematic representation of cationic vacancies in Ni:O (*a*) ■ undissociated vacancy, (*b*) ◩ singly dissociated vacancy, (*c*) □ doubly dissociated vacancy.

problem in heat conduction (8), we obtain for the steady-state concentration,

$$c/c_0 = 1 + (k_2/D_i)\,(y - x)/1 + (k_2/D_i)y.$$

Hence the rate of growth of the film,

$$dy/dt = -(n_i + c_y)^{-1}D_i(\delta c/\delta x)$$
$$= (n_i + c_y)^{-1}(k_2/D_i)c_0/1 + (k_2/D_i)y.$$

Since $n_i >> c_y$,

$$dy/dt = (k_2c_0/n_iD_i)/\ 1 + (k_2/D_i)y. \quad \text{(XIV)}$$

This has the form of equation (III), and on integration with the initial condition $y = 0$ at $t = 0$,

$$y = (2c_0/n_i)\ t/y - 2D_i/k_2\,. \quad \text{(XV)}$$

The above expressions are all based on the diffusion of uncharged particles, whereas in a growing oxide film the diffusing species is more likely to be an ion. This problem has been discussed by Mott and Gurney (9). The results for low temperatures and thin films show many interesting special features (10), but the only result we require is that applicable to thick films and high temperatures, where the net effect of the space charge is to introduce a factor of 2 (for completely dissociated defects and electrons) into the relation between parabolic rate constant and diffusion coefficient. Thus, instead of equation (XII), we have

$$k_1 = 2D_i\,(f_0 - f_1). \quad \text{(XVI)}$$

DEFECTS IN OXIDES

The diffusion of ions through the oxide films is greatly facilitated by the occurrence of defects in the oxide structures, such as interstitial ions and vacancies. In most cases, the mobility of the defects is so much higher than that of ions in normal lattice positions that the entire observed diffusion can be ascribed to the defects.

The defects can be divided into two classes, stoichiometric and nonstoichiometric. The former are those described by Frenkel and Schottky. The nonstoichiometric defects are the results of solution of an excess of metal or of oxygen in the oxide. An excess of metal can occur through an interstitial solution of metal atoms (which may be dissociated to ions and electrons), or through vacancies in some of the normal oxide-ion sites with electrons attached to the positive hole (and these complexes may be entirely or partially dissociated). An excess of oxygen can dissolve in the oxide either in the form of interstitial oxygen atoms (possibly dissociated) or in the form of vacant cation sites with a corresponding number of electrons removed from neighboring ions. In Fig. 2, these cation vacancies are shown for the case of nickel oxide.

We shall consider a few examples that are of special importance in the study of high temperature oxidation rates.

Zinc Oxide

If zinc oxide is prepared by the thermal decomposition of zinc oxalate, or by the complete oxidation of zinc in oxygen, it has an extremely low electrical conductivity, of the order of 10^{-7} ohm^{-1}cm^{-1} at 25°C. If this material is heated in air at 1000°C and then cooled, its conductivity is greatly enhanced to about 10^{-2} (11).

It has usually been assumed that the increased conductivity is caused by the formation of interstitial zinc atoms (Zn_i) according to the following reactions (12):

$$\text{ZnO (c)} = \text{Zn (g)} + \tfrac{1}{2}\,\text{O}_2 \qquad (A)$$
$$\text{Zn (g)} = \text{Zn}_i \qquad (B)$$
$$\text{ZnO (c)} = \text{Zn}_i + \tfrac{1}{2}\,\text{O}_2\,. \qquad (C)$$

The standard free energy of reaction (*A*), ΔF^0_1, can be obtained from the measured equilibria in the reduction of ZnO by CO or H_2 (13). The ΔF^0_2 of reaction (*B*) can be calculated from the partition function of zinc vapor as an ideal monatomic gas, and that of the interstitial zinc as an ideal solute in the zinc oxide crystal. The result obtained for the mole fraction f of interstitial zinc atoms in equilibrium with zinc vapor at 1 atm is

$$-\ln f = (U/RT) + \ln (2\pi m\nu^2)^{3/2} (kT)^{-1/2} A. \quad \text{(XVII)}$$

Here U is the energy necessary to transfer a zinc atom from the vapor to an interstitial position; ν is the vibration frequency of the interstitial zinc atom; m is the mass of a zinc atom; and A is a conversion factor from cc atm to ergs. A convenient notation for small fractions of defects is to write $pf = -\log f$, so that equation (XVII) becomes

$$pf = U/4.57T + \log (2\pi m\nu^2)^{3/2} (kT)^{-1/2} A. \quad \text{(XVIII)}$$

In order to calculate the concentration of interstitial zinc from the over-all reaction (C), it is necessary to add $\Delta F_1^0/4.57T$ to the pf in equation (XVIII).

An estimate of U can be obtained as follows. The structure of zinc oxide is based on a hexagonal closest packed array of oxide ions, with zinc ions occupying half the tetrahedral holes. Let us assume that interstitial zinc atoms enter the octahedral holes. These have a radius of 0.67 Å, whereas the radius of the zinc atom in metallic zinc is 1.39 Å. The energy U_0 to introduce a sphere of radius a_1 into a smaller spherical hole of radius a_2 in an isotropic elastic medium (14) can be calculated from the formula,

$$U_0 = \frac{6\pi a_2^3}{(\alpha + 1)\beta_1} (\Delta/a_1)^2 \quad \text{(XIX)}$$

with

$$\alpha = (1 + \gamma_2)/2(1 - 2\gamma_2)\, a_2\beta_2/a_1\beta_1 .$$

Here β_1 is the compressibility of zinc, 1.7×10^{-6} cm^{2}kg^{-1}; β_2 is the compressibility of zinc oxide, 0.75×10^{-6}; $\Delta = a_2 - a_1$; γ is Poisson's ratio for ZnO, taken to be 0.25. The estimated contribution to U is then 10 kcal/mole. This figure will be lowered by the Van der Waals attraction between the zinc atom and the surrounding oxide ions, which can be estimated from the London equation,

$$E_0 = -(3/2)\, I_a I_b/(I_a + I_b)\, d_A d_B/r^6.$$

The I's are the ionization potentials, the d's the polarizabilities, and r is the internuclear separation. In this case, $I_{Zn} = 9.4$ ev, $I_{O^-} = 54.8$ ev, $d_{Zn} = 2.00$, and $d_{O^-} = 2.75 \times 10^{-24}$ cc; $r = 2.80$ Å. Thus $E_0 = 0.125$ ev/pair, or 17 kcal for the six oxide ions surrounding an octahedral hole.

From the elastic distortion and the Van der Waals terms, therefore, $U = -7$ kcal, an estimate subject to uncertainty but probably of the right order. It is unlikely that ν is less than 10^{12}, and this figure will be used in the calculation of pf. The results are shown in Fig. 3. Curve A is the equilibrium value of Zn_i from the reaction $ZnO = Zn_i + \frac{1}{2}O_2$, with an oxygen pressure of 0.2 atm. Curve B gives the concentrations of Zn_i in equilibrium with zinc vapor at 1 atm, and curves C and D, the concentrations in equilibrium with liquid zinc and solid zinc, respectively.

The extent of dissociation of interstitial zinc atoms into ions and electrons is indicated by the electrical conductivity σ of zinc oxide. There seems to be general agreement that plots of log σ vs. T^{-1} can be represented by two straight lines (15). The temperature coefficient of σ in the low temperature region (about 25°C) may be ascribed to the thermal excitation of an electron from the interstitial zinc atom into a "conduction band," $Zn_i = Zn_i^+ + e$. The concentration of electrons from such a dissociation can be calculated (16) from the equation,

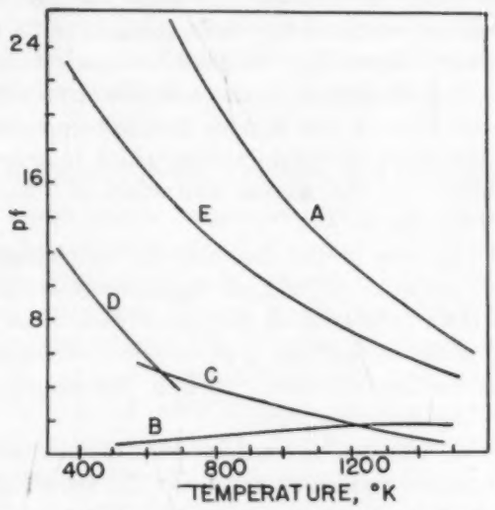

FIG. 3. Calculated fractions of interstitial atoms or ions in zinc oxide. (A) Interstitial Zn in ZnO in equilibrium with air; (B) in equilibrium with zinc vapor at 1 atm; (C) in equilibrium with liquid zinc; (D) in equilibrium with solid zinc; (E) interstitial Zn^+ ions in ZnO in equilibrium with air.

$$n(N - n)^{-1/2} = 2V^{1/2} (2\pi\, mkT/h^2)^{3/4} \exp(-E_1/2kT)$$
$$= 4.55 \times 10^8\, T^{3/4} \exp(-E_1/2kT). \quad \text{(XX)}$$

Here n is the number of electrons, N is the number of donor atoms, V is the volume of the crystal, m is the electronic mass, and E_1 is the energy difference between the donor level and the conduction band. For $\frac{1}{2} E_1$ we may take the activation energy of the low temperature conductivity, about 5.5 kcal (11).

It is worthwhile to notice the structural factors that determine the value of E_1. We may write $E_1 = e_1 + e_2 + e_3 + e_4$. The e_1 is the Madelung energy of the Zn_i^+ ion, which can be calculated readily by the method of Frank (17). The e_2 is a distortion energy provided by the fact that the ion occupies less volume than the atom. The e_3 is the

energy to remove the electron from the atom, which may be set equal to I_1/κ^2, with κ the dielectric constant of ZnO, and I_1 the first ionization potential of Zn. The e_4 is the polarization energy e_p. Introducing the values for these quantities, we obtain $E_1 = 11 = 25 - 9 + 2 - e_p$, so that the polarization energy can be estimated as 7 kcal.

Combining equations (XVIII) and (XX), we obtain

$$pf^+ = \tfrac{1}{2}pf + 3.23 - \tfrac{3}{4}\log T + E_1/9.14T \quad \text{(XXI)}$$

where f^+ is the equilibrium mole fraction of Zn_i^+. The values of pf^+ from this equation are shown in curve E of Fig. 3.

The observed activation energy for the high temperature conductivity varies from 16 to 28 kcal, apparently depending on the concentration of donors. It is likely that at temperatures up to 1000°K the production of new donors does not appreciably affect the observed conductivity, which is probably determined by the second ionization of "frozen" interstitial atoms.

The response of the conductivity to changes in oxygen pressure is almost instantaneous above 770°K (18). It is evident that adsorption of oxygen on the oxide surface can provide effective traps for the conduction electrons, with a consequent fall in the conductivity (19).

It is of interest to consider why dissociation of ZnO does not give anion vacancies $\square_a$, according to

$$2ZnO = 2Zn^+ + \square_a + \tfrac{1}{2}O_2 .$$

The ΔH for this reaction can be estimated from the following steps:

$$\begin{aligned}
O^-(c) &= O^-(g) + \square_a && e_m - e_p \\
O^-(g) &= O + 2e && A_1 + A_2 \\
O &= \tfrac{1}{2}O_2 && D/2 \\
2e(g) + 2Zn^{+2}(c) &= 2Zn^+(c) && e_m - 2e_p' - 2I_2 .
\end{aligned}$$

$$\text{Thus} \quad \Delta H = 2e_m - (e_p + 2e_p') - \frac{D}{2} - (A_1 + A_2) - 2I_2 = 963 - (e_p + 2e_p').$$

With the reasonable estimates (20, 21), $e_p' = 160$, $e_p = 450$, $\Delta H = 193$ kcal, which is considerably larger than the ΔH for forming interstitial zinc atoms. If the $\square_a$ were formed by solution of Zn(c) in ZnO, the ΔH would be lowered, by the heat of formation of ZnO, to 193 − 83 = 110 kcal.

In crystals such UO_2, however, there is evidence that anion vacancies do occur, with U^{+3} ions to preserve electrical neutrality (22). The transition $U^{+4} \rightarrow U^{+3}$ releases more energy than $Zn^{+2} \rightarrow Zn^{+1}$. One may, in general, expect to find anion vacancies in oxides in which the metal ion bears a charge of +4 or more.

We have not considered stoichiometric defects in this discussion. They will, of course, occur to some extent, but their formation requires much more energy than that of interstitial excess ions. Consider, for example, the energy E_3 required to move a zinc ion from a normal lattice site to an interstitial position, leaving a vacant cation site. $E_3 = e_m - e_p + e_i$. The e_m is the Madelung energy of ZnO; e_p is the polarization energy of the positive vacancy; and e_i is the energy of the interstitial Zn_i^{+2} relative to that of the gaseous ion. For ZnO e_m is 970 kcal; and e_i is about 50. From the calculations on CaO and MgO (20) it is unlikely that e_p is more than 450 kcal. Thus E_3 is about 570 kcal. This energy is so much higher than the energy of formation of excess Zn_i^{+2}, that we can ignore such stoichiometric defects. A similar conclusion will probably be valid for all stoichiometric defects in oxides that involve the removal of a multiply charged ion from a normal to an interstitial position.

Another possibility is that defects in ZnO might occur through the formation of vacant anion sites with a pair of singly charged Zn_i^+ ions to preserve electrical neutrality. Such a defect would appear to be most unlikely from an energetic standpoint since it would involve the loss of the large Madelung energy with the recovery of even less polarization energy than in the Frenkel type with cation vacancies.

Beryllium Oxide

Few data are available on defects in BeO, which has the same structure as ZnO. It is interesting, however, to predict from the thermodynamic data the relative concentrations of Be_i^{+2} ions and Zn_i^{+2} ions. The heat of sublimation of Be at its melting point is 78 kcal, compared to 31 kcal for Zn. Considering this predominant factor alone, we should expect the concentration of Be_i^{+2} to be less than that of Zn_i^{+2} for the oxides in equilibrium with the solid metals by a factor of $\exp(78\text{-}31)/3RT$, or about 6×10 at 1000°K. For interstitial ions arising from the dissociation reaction, the difference in ΔF_1^0 between ZnO and BeO would introduce a factor of $\exp(102/3RT)$ at 1000°K, or about 6×10^7.

Cuprous Oxide

The discussion of the formation of interstitial atoms and ions given for ZnO can be applied also to Cu_2O. The reaction $Cu_2O = \tfrac{1}{2}O_2 + 2Cu_i^+ + 2$ would in fact have a lower ΔF^0 than the corresponding ZnO reaction, so that one might at first expect a considerable concentration of interstitial Cu_i^+ in the oxide in equilibrium with air. On the other hand, the vapor pressures of solid and liquid copper are much lower than those of zinc, so that the concentration of interstitial copper in the oxide

in equilibrium with the metal would be much lower than in the case of Zn-ZnO.

Interstitial copper is not actually found in Cu_2O in equilibrium with air, because the solution of excess oxygen in the oxide is a more favorable reaction:

$$\tfrac{1}{2}O_2 + Cu_2O = 2Cu^{+2} + 2\square_c + 2O^{=} \quad (D)$$

where $\square_c$ denotes a vacant cation site. If the vacancies produced by this reaction are more numerous than the interstitial ions, the latter at equilibrium will be virtually annihilated by the reaction $Cu_i^{+} + \square_c = Cu^{+}$. This is simply the reverse of the reaction leading to stoichiometric Frenkel defects, which has a low equilibrium constant. One factor that favors a reaction like (*D*) for Cu_2O as compared to ZnO is the relative ease of formation of the Cu^{+2} ion: $Cu^{+} = Cu^{+2} + e - 20.3$ ev; $Zn^{+2} = Zn^{+3} + e - 40$ ev. It is necessary, however, to divide these ionization potentials by κ^2, about 40, so that this contribution to the energy difference would appear to be only about 0.5 ev or 12 kcal. Thus the energetic factors for excess metal and for excess oxygen are often closely balanced. The entropy factor favors loss of oxygen from the oxide rather than solution of oxygen in the oxide, and at 1000°K this difference in $T\Delta S$ may amount to 20 to 40 kcal. It has been found that Cu_2O heated in O_2 contains excess oxygen, whereas Cu_2O heated in vacuum may contain excess copper (23). Although ZnO heated in air contains excess zinc, it is likely that in oxygen at high pressure, or in equilibrium with energetic oxygen species such as O_3 or O_2^{+}, ZnO would dissolve excess oxygen, with a formation of Zn^{+3} or O^{-} ions to preserve electrical neutrality.

The most accurate measurements of the oxygen excess in Cu_2O appear to be those of Wagner and Hammen (24). The pressure dependence of the solubility from their data is as $P_{O_2}^{1/5}$, whereas from equation (*D*), with practically complete association of vacancies and positive holes, we should expect a $P_{O_2}^{1/4}$ dependence. From their data one obtains $\Delta H^0 = 7.4$ kcal for the heat of formation of one *associated* cation vacancy. The concentration of associated vacancies in equilibrium with air is given by the empirical equation,

$$pf = (7400/4.57T) + 1.82. \quad \text{(XXII)}$$

The activation energy E for the high temperature conductivity of Cu_2O is from 8 to 18 kcal. The E may be set equal to $\tfrac{1}{2}\Delta H^0 + \tfrac{1}{2}U$, where U is the energy required to free the trapped positive hole. Thus U is about 20 kcal.

The experimental ΔH for vacancy formation can be used to obtain an estimate of the polarization energy at the vacancy and the Cu^{+2} site, by means of the following cycle:

$$\begin{aligned}
Cu^{+}(c) &= Cu^{+}(g) + \square_c & e_m - e_p \\
Cu^{+}(c) &= Cu^{+2}(c) + e & I_2 - e_m - e'_p \\
Cu^{+}(g) + e &= Cu\,(g) & I_1 \\
Cu(g) + \tfrac{1}{4}O_2 &= \tfrac{1}{2}Cu_2O & e_f \\
\tfrac{1}{2}Cu_2O + \tfrac{1}{4}O_2 &= Cu^{+2} + \square_c + O^{=} & \\
& \Delta H = I_2 - I_1 - e_p - e'_p - e_f.
\end{aligned}$$

Introducing the experimental quantities, we obtain $27 = 470 - 179 - 102 - (e_p + e'_p)$, or $e_p + e'_p = 162$ kcal. Calculations for NaCl (20, 21) indicate that the e_p at a vacant Na^{+} site is 56 kcal if the ions are held rigidly in place, or 110 kcal if the ions are free to move to new equilibrium positions. It is reasonable that e_p should be lower in the Cu_2O structure, for a Cu^{+} site has two $O^{=}$ neighbors at 3.01 Å, compared with the six Cl^{-} neighbors at 2.31 Å of Na^{+} in NaCl.

Manganous, Ferrous, Cobaltous, and Nickelous Oxides

These oxides behave as typical *p*-type semiconductors, with an excess of oxygen and vacant cation sites. Ferrous oxide is not stable below 560°C, decomposing into Fe and Fe_3O_4; and the FeO structure may contain a large excess of oxygen, up to 1.3 atom per cent in equilibrium with iron, or from 1.9 (700°C) to 3.5 (1300°C) atom per cent in equilibrium with magnetite (25, 26). The solution of oxygen can be represented by

$$2M^{+2} + \tfrac{1}{2}O_2 = O^{=} + \square_c + 2M^{+3}\,(O^{-}). \quad (E)$$

The question of whether the positive hole resides on metal ions, on oxide ions, or on both, must in this case be considered in some detail, since removal of an electron from an M^{+2} ion is related to the third ionization potential, as compared to the considerably easier process in cuprous oxide, which is related to the second ionization potential of copper.

The energies required to abstract an electron from M^{+2} and $O^{=}$ can be estimated on the basis of an ionic model for the oxide structures by consideration of the following two cycles: (*a*) removal of M^{+2}; $M^{+2} = M^{+3} + e$; replacement of M^{+3} in solid. The net result is the removal of an electron from an M^{+2} ion in the crystal, and the required energy is $W_m = I_3 - e_m - e'_p$, the e'_p being the polarization energy resulting from replacement of an M^{+2} by an M^{+3} in the crystal. (*b*) Removal of $O^{=}$; $O^{=} = O^{-} + e$; replacement of O^{-} in solid. The net result is the removal of an electron from an $O^{=}$ in the crystal, and the required energy is $W_o = e_m - A_2 - e''_p$, the e''_p being the polarization energy resulting from replacement of an $O^{=}$ by an O^{-}, and A_2 the electron affinity of O^{-}. The numerical values in ev are summarized in Table I, the polarization

energies being estimated from the rigid structure calculations on oxides having the same crystal structure (20). These estimates indicate that it is somewhat easier to remove an electron from an M^{+2} than from an O^{-}, thus supporting the usual picture (27) that the positive hole is an M^{+3} ion. It must be remembered, however, that the K series of x-ray emission spectra from such oxides (28) displays a broad band, about 10 to 15 ev wide, which has usually been attributed (29) to transitions from what is called the "2p band of the oxide ions" to the vacant K level in the oxide ions. The band width is much larger than the probable energy differences between W_m and W_o, and it seems likely that the band contains electrons from both the metal and the oxygen. One might call the positive hole a hybrid of $Ni^{+3}O^{-}$ and $Ni^{+2}O^{-}$ structures. The trapping of the positive hole at the site of the cation vacancy would not significantly alter this picture, since the activation energy required to release the trapped hole is less than 2 ev [NiO(30)]. There is

TABLE I

	MnO	FeO	CoO	NiO
I_3	33.7	30.6	33.5	35.4
e_m	20.5	20.7	20.9	21.1
e_p'	4.2	4.3	4.4	4.5
A_2	6.5	6.5	6.5	6.5
e_p''	2.9	2.8	2.7	2.6
W_m	9.0	5.6	8.2	9.8
W_o	11.1	11.4	11.7	12.0

an experimental value of the thermionic work function of NiO of about 4.5 ev (31), a figure consistent with the removal of an electron from the top of a band 10 ev wide, whose center lies at about -10 ev, as in Table I.

We may now consider the energies ΔH to form cation vacancies in FeO, CoO, and NiO. In the case of FeO, the experimental value (26) of ΔH for the solution of one atom of oxygen from O_2 into the FeO phase is -56 kcal at 25°C. If the figure is compared with a ΔH calculated from the usual cycle, the polarization energy $e_p + e_p'$ can be estimated as 437 kcal, which is about half the Madelung energy. The estimated heats of formation of vacancies in CoO and NiO by solution of oxygen from O_2 would be -23 and -14 kcal, respectively. These figures refer to undissociated vacancies.

Cationic Diffusion Coefficients in the Oxides

The diffusion of cations in oxides like those under consideration proceeds almost entirely by way of the defects. Thus the cationic diffusion coefficient D can be written (32) to a very good approximation as the diffusion coefficient for a defect D_i times the probability of finding a defect, i.e., the defect fraction f_i,

$$D = D_i f_i . \qquad \text{(XXIII)}$$

If the solid is in equilibrium with its environment, the defect fraction is an equilibrium quantity, which can be related to the standard free energy of formation of defects, or calculated by statistical thermodynamics. In some cases, however, the f_i may have a nonequilibrium value as the result of "freezing" of defects produced at higher temperatures.

The defect diffusion coefficient D_i can be related to the difference in free energy between an initial configuration and one at the saddle point between two free energy minima a distance d apart. Thus Eyring (33) has obtained

$$D_i = (RTd^2/Nh) \exp (\Delta S_i^*/R) \exp (-\Delta H_i^*/RT). \qquad \text{(XXIV)}$$

A typical equation for the formation of defects in a p-type oxide was equation (E), for which the equilibrium constant can be written as

$$K = (+)^2(\square_e)P_{O_2}^{-1/2},$$

so that for completely dissociated vacancies and positive holes, $(\square_e) = K^{1/3}P_{O_2}^{1/6}$. In this case, therefore,

$$f_i = \exp (\Delta S^0/3R) \exp (-\Delta H^0/3RT)P_{O_2}^{1/6} .$$

The general form of equation (XXIII) for D therefore becomes:

$$D = (RTd^2/Nh) \exp [(n^{-1}\Delta S^0 + \Delta S_i^*)/R] \exp [(n^{-1}\Delta H^0 + \Delta H_i^*)/RT]P_{O_2}^{1/n} . \qquad \text{(XXV)}$$

The n is an integer equal to the number of particles formed by dissociation of the defect. A similar expression is found for an n-type oxide, except that the ΔS^0 and ΔH^0 refer to the formation of an interstitial metal ion.

In order to separate the two factors in D, an independent determination of the variation of defect concentration with temperature is necessary. Then one can evaluate ΔS^0 and ΔH^0, and hence the ΔS_i^* and ΔH_i^* for the defect mobility.

The D_i for defects is expected to have a small ΔS_i^*, probably slightly positive (34, 35). A large negative ΔS_i^* for defect mobility strongly indicates short-circuiting diffusion paths, such as those provided by grain boundaries. The effective diffusion coefficient in a polycrystalline material will then depend on the fraction of the cross-sectional area that is occupied by the grain boundaries. For example, with a grain diameter r, and an effective grain-boundary diameter δ (36), the fraction of open area

would be $2\delta/r$. With $\delta = 5$ Å and $r = 100$ Å, the factor is 10^{-1}; with $r = 1000$ Å, 10^{-2}, etc. Thus, in grain-boundary diffusion the effective activation entropy is lowered by $-R \ln (2\delta/r)$.

In metal-oxide systems, we must consider the possibility that both the metal and the oxygen may diffuse along the grain boundaries. In contrast with the situation in metals, however, the ΔH^0 term in equation (XXV) is probably about the same for the grain boundary and the volume formation of defects, so that a major energetic factor in favor of the boundary process does not occur in oxides, so far as metal diffusion is concerned. In oxides without anion vacancies, oxygen diffusion would seem certainly to occur preferentially along the boundaries, perhaps as atomic oxygen. This process will be important in metal oxidation, however, only if it has a rate comparable to or greater than that of the metal diffusion.

Diffusion measurements have been made with radioactive copper in cuprous oxide (37) and radioactive zinc in zinc oxide (38). The copper diffusion was followed in strips of oxide made by the oxidation of spectroscopically pure copper. The surface of the Cu_2O strip was coated with an extremely thin layer of active copper, and the diffusion proceeded at 800° to 1000°C and 10^{-2} cm oxygen pressure. The self-diffusion coefficients could be represented by $D = 0.044 \exp(-36 \text{ kcal}/RT)$ cm^2 sec^{-1}. The D at 1000°C is in excellent agreement with a value calculated from the conductivity data of Wagner (1) by means of the Einstein relation $D = kT\theta\sigma/e^2n$, where θ is the transference number of the Cu^+ ions, e is the electronic charge, and n is the number of Cu^+ ions in a cc of Cu_2O. This agreement indicates that there is no diffusion of copper via uncharged species, such as trapped vacancies.

It is desirable to tabulate diffusion results in oxides under standard conditions, and for a p-type oxide like Cu_2O the best choice for a standard state would appear to be at one atmosphere oxygen pressure. The D's recorded in Table II have been reduced to the standard state under the assumption that they depend on the seventh root of the oxygen pressure, as the conductivities do. The average vacancy concentrations from equation (XXII) are also included in the table. Since $D = D_i f_i$, it is possible to separate the vacancy diffusion coefficients D_i. In the last column of the table is listed the time τ for the vacancy concentration at the center of a 0.02-cm thick slab of oxide to fall to one-tenth of its initial value, after the concentration at the surface is reduced to zero (for example, by exposure of the oxide strip to vacuum). These figures are of interest in connection with the frequently used concept of "frozen defects." In this case, which is probably typical of many p-type oxides, the freezing of vacancies would not be expected until quite a low temperature is reached. It should be noted that τ depends on the square of the thickness of the slab.

If the over-all diffusion coefficients are fitted to equation (XXV), with the use of equation (XXII) to give ΔH^0 and ΔS^0, and $d = 3.05$ Å, $n = 2$, one obtains: $\Delta H^0 = 7.4$ kcal; $\Delta S^0 = -8.0$ cal deg^{-1}; $\Delta H_i^* = 30.1$ kcal; $\Delta S_i^* = 4.6$ cal deg^{-1}. The ΔH^0 and ΔS^0 refer to the formation of undissociated vacancies; the negative ΔS^0 represents the loss of entropy when gaseous oxygen dissolves in the oxide. The ΔH_i^* and ΔS_i^* are in a sense still composite terms, since the vacancy must dissociate before it becomes mobile. The observed ΔH_i^* is made up of about 12 kcal for the dissociation energy and 18 kcal for the activation energy of mobility of the free vacancy.

Disks of ZnO were prepared by sintering the compressed powder. The radioactive zinc was deposited in thin layers, and the decline in surface activity was measured as a function of time and temperature. The measurements were made in air from 1100° to 1600°K, and the results can be summarized in the equation $D = 1.5 \exp(-74 \text{ kcal}/RT)$ cm^{2}sec^{-1}. Thus $\Delta H^* = 72$ kcal.

TABLE II. *Diffusion of copper and cation vacancies in cuprous oxide*

(Standard pressure = 1 atm O_2)

Temp, °C	f_i	D, cm^{2}sec^{-1}	D_i, cm^{2}sec^{-1}	τ, sec
1000	1.0×10^{-3}	9.7×10^{-8}	9.7×10^{-5}	1.1
900	7.9×10^{-4}	2.8×10^{-8}	3.5×10^{-5}	3.0
800	5.9×10^{-4}	7.2×10^{-9}	1.2×10^{-5}	8.6
600	2.6×10^{-4}	1.5×10^{-10}	5.8×10^{-7}	181
400	7.4×10^{-5}	3.9×10^{-13}	5.3×10^{-9}	2.0×10^4
200	6.7×10^{-6}	3.5×10^{-16}	5.2×10^{-13}	2.0×10^8

The ΔH^0 for the formation of interstitial Zn_i^{+2} has been estimated for reactions (A), (B), and (C) above. $\Delta H^0 = 110 - 7 + 11 + 40$. The first term is the heat of the dissociation of $ZnO = Zn(g) + \frac{1}{2}O_2$; the second term is the heat of solution of zinc atoms in interstitial positions in the oxide; the last two terms are the heats of the first and second ionizations of interstitial zinc atoms. Since $\Delta H^* = \Delta H_i^* + (\Delta H^0/3)$, we obtain the activation heat for the mobility of interstitial Zn_i^{+2} as $\Delta H_i^* = 21$ kcal. The rather low ΔH_i^* appears reasonable when it is recalled that the zinc oxide structure contains a series of channels parallel to the hexagonal axis and joining successive octahedral holes.

If the diffusion of zinc was studied in zinc oxide in equilibrium with solid or liquid zinc, the activation energy would be considerably lower, since the interstitial zinc would then be formed, not by the highly endothermic dissociation of the oxide, but by solution of zinc from the solid or liquid. The expected

heat of activation would be $\Delta H^* = \Delta H_i^* + (\Delta H^{0\prime}/3)$, where $\Delta H^{0\prime}$ is the heat of vaporization of zinc plus the heat of solution of the zinc vapor in the oxide to yield interstitial ions. Thus $\Delta H^{0\prime} = 30 + 44 = 74$, and $\Delta H^* = 46$ kcal.

Parabolic Rate Constants

The numerical values of the parabolic rate constants may now be analyzed in terms of the preceding discussion of defect concentrations and diffusion coefficients. The most reliable data are summarized in Table III.

TABLE III. *Parabolic rate constants for metal oxidation*

Temp range, °C	Metal	Oxide	ΔH^*	ΔS^*	Reference
p-type oxides with cation vacancies					
800–1000	Cu	Cu_2O	33.8	0.5	(37)
			35.5	−0.3	(39)
500–1000	Ni	NiO	34.7	−17.0	(40)
700–1000			35.0	−10.5	(41)
700–1000	Co	CoO	36.3	−10.0	(42)
700–950	Fe	FeO*	22.4	8.6	(43)
400–600	V	V_2O_3	30.7	−7.2	(45)
350–450	Mo	MoO_2	36.5	0.5	(44)
n-type oxides with interstitial metal					
360–400	Zn	ZnO	28.5	−22.6	(46)
350–450	Al	Al_2O_3	21.4	−28.6	(47)
750–950	Be	BeO	50.3	−7.5	(50)
			59.5	−3.4	(51)
700–900	Cr	Cr_2O_3	66.3	+12.0	(52)
500–900	Zr	ZrO_2	32.0	−7.1	(50)
400–500	W	WO_3	45.7	11.0	(44)
250–450	Ta	Ta_2O_5	27.4	−10.0	(53)
n-type oxides with anion vacancies					
200–425	Zr	ZrO_2	16.8	−27.3	(49)
350–600	Ti	TiO_2	24.3	−22.8	(48)

* Outer layer Fe_3O_4.

P-Type Oxides

In these cases, which include copper, iron, cobalt, and nickel, the oxide contains an excess of oxygen with associated cationic vacancies. Diffusion coefficients measured in the oxides exposed to air or reduced oxygen pressures should be directly comparable with parabolic constants measured under the same conditions, since in both the diffusion and the metal oxidation the cation vacancies are formed by the same process, the solution of oxygen at the oxide-oxygen interface.

From equation (XVI), since $f_0 \gg f_1$, $k_1 = 2D_i f_0$. If f_0 is the equilibrium defect concentration, one obtains from equation (XXIII)

$$k_1 = 2D. \qquad \text{(XXVI)}$$

This relation applies when the rate constant and the diffusion coefficient refer to the same oxygen pressure. This relation is closely followed by the experimental data on copper oxidation and diffusion of radiocopper in cuprous oxide (37).

Consider next the growth of FeO on Fe. In all the work so far reported, the oxygen pressure has been such that the oxide film was composed of at least two layers. In the case cited in Table III, the inner layer was FeO and the outer one Fe_3O_4. The microscopically measured thickness of the FeO layer yielded the parabolic rate constants given in the table. From the iron-oxygen phase diagram (25, 26) it is known that the ΔH to transfer an oxygen atom from Fe_3O_4 to FeO is close to zero. Hence, the observed $\Delta H^* = 22$ kcal must be simply the mobility of a cation vacancy in FeO. Since the ΔS for the formation of the vacancy in FeO by solution of oxygen from Fe_3O_4 is, of course, also about zero, the observed positive ΔS^* for the oxidation rate also represents the mobility term alone. This is the normal positive entropy of activation that would be expected owing to the increased randomness attendant on the passage of a cation from a normal site to the saddle point. It may also include a contribution from the dissociation of the vacancy.

In the case of NiO, there is no outer layer of higher oxide, and the equilibrium vacancy concentration at the NiO-O_2 interface is maintained by solution of oxygen from the gas. In Cu_2O the solution of $\frac{1}{4}O_2$ is required for each vacancy, whereas in NiO, $\frac{1}{2}O_2$ is required. Since the entropy of gaseous oxygen is about 48 cal deg^{-1} per mole, a considerable contribution to the negative ΔS^* for nickel oxidation is due to this factor. We do not yet know, however, whether cationic diffusion in nickel oxide proceeds through singly dissociated or doubly dissociated vacancies.

N-Type Oxides

In the cases of zinc, aluminum, beryllium, and chromium, the excess of metal most probably occurs in interstitial positions. Diffusion coefficients measured in the oxides exposed to oxygen cannot be directly compared with the parabolic rate constants, since the excess metal in the oxide, in the one case, comes from a dissociation of the oxide, and, in the other case, from solution from the underlying solid metal. In absence of underlying metal Cr_2O_3 is a *p*-type oxide.

In the case of zinc oxide, it was shown how the ΔH^* for diffusion in air, 72 kcal, would be reduced to 46 kcal for diffusion in ZnO in equilibrium with solid Zn. Even this figure, however, is markedly higher than the observed $\Delta H^* = 29$ kcal for the parabolic rate constant. This ΔH^* is coupled with a

large negative ΔS^*, and in fact the parabolic rate constants for Zn, Al, Ti, and Zr all share this peculiarity of a low ΔS^*. It may be noted also that in all these cases the oxidation rate has been measured at a comparatively low temperature and with thin oxide films.

The parabolic rate constants for Be and Cr have normal ΔS^* and rather large ΔH^*. The ΔH^* of 55 for BeO should be predictable from the observed diffusion data on ZnO, since ZnO and BeO have the same crystal structures. The heat of sublimation of Zn is 30 kcal, and that of Be is 78 kcal. This difference would lead to an increase in ΔH^* for the Be diffusion of $48/3 = 16$, so that if this were the only factor involved, the ΔH^* for Be oxidation would be $45 + 16 = 61$ kcal, instead of the observed 55. The 6 kcal difference may be ascribed to the larger polarization energy of the Be^{+2} ion as compared to Zn^{+2}, as well as to a slightly lower activation energy for mobility, due to the smaller size of the Be^{+2}.

No data are available on the Cr-Cr_2O_3 system that would permit an analysis of the observed ΔH^*. If the diffusing species is an interstitial Cr^{+3} ion, one would expect it to be highly mobile. The large ΔH^* would then be due to the heat of sublimation of chromium, a contribution of $84/4 = 21$ kcal from this source; and the energy required to strip three electrons from the interstitial Cr, about 31 kcal from this source; and about 15 kcal for the mobility activation energy. There is as yet no way of deciding, however, whether diffusion of Cr^{+2} ions, or even Cr^{+}, might not be a more favorable process.

When one returns to Zn, Ti, Al, and Zr, the most puzzling problems in all the oxidation kinetics are encountered. Al follows an exponential type of law below 300°C as does Zn below 350°C. The range of validity of the parabolic law is limited at higher temperatures, for zinc by the melting point at 420°C, for aluminum and titanium by transitions to a linear law at 500° and 750°C, respectively. Titanium oxidation is further complicated by solution of oxygen in the metal. The zirconium case is particularly instructive, since it exhibits a normal diffusion behavior at high temperatures and an extremely low ΔS^* at low temperatures.

The apparently attractive hypothesis that the low ΔH^* and large negative ΔS^* for these reactions indicate grain-boundary diffusion of metal does not withstand closer analysis. The crystallite size in the Al_2O_3 film on Al is so small that no electron diffraction pattern is observed (44), and in the case of ZrO_2 on Zr the crystallite size is probably about 100 Å (50). Thus it is difficult to see how the effective ΔS^* could be lowered by a grain-boundary diffusion by more than about 8 cal deg^{-1}. Diffusion of oxygen ions via anion vacancies, or of oxygen atoms via grain boundaries would provide a mechanism of large negative ΔS^*. In ZrO_2 and TiO_2 anion vacancies would be energetically likely. The adsorption of oxygen from the gas is associated with an entropy loss of about 20 cal deg^{-1} per anion vacancy in these cases. Further experimental work on the diffusion coefficients of anions and cations in these oxides is required to prove this mechanism.

In the case of zinc oxidation, at least five different mechanisms have been suggested: (*a*) diffusion of oxygen inward along grain boundaries (54); (*b*) diffusion of oxygen via anion vacancies; (*c*) diffusion outward of interstitial zinc (55); (*d*) outward migration of interstitial zinc caused by the electric field of surface oxide ions (56); (*e*) a rate-controlling reaction at the oxide-oxygen interface (57). A possible reason for the diverse interpretations might be that not all observers were studying the same process, since the oxidation rate of zinc is very sensitive to the pretreatment of the surface. Thus, 40-hr exposure to oxygen at 400°C can produce about 100 Å of ZnO if the zinc is first "passivated" by dipping in concentrated nitric acid, or about 1000 Å of ZnO if the zinc is first oxidized for 10 hr at 300°C, or about 5000 Å of ZnO if electropolished zinc is exposed directly to oxygen at 400°C.

Measurement of diffusion of radioactive zinc during oxidation should allow one to decide between mechanisms (*a* or *b*), (*c* or *d*), and (*e*). It is unlikely that a distinction could be made between (*c*) and (*d*).

The test cannot be made by the technique used for copper oxidation (58, 59), because the self-diffusion coefficient of zinc at 400°C is much larger than the diffusion coefficient of zinc in ZnO. The procedure used, therefore, was first to oxidize the zinc foil to about 1000 Å of ZnO. It was then rinsed in water, wiped free of excess water, suspended briefly in ammonia vapor, dipped into a solution of radioactive zinc acetate, rinsed in water, and dried. This treatment produced a thin layer of radioactive $Zn(OH)_2$ on the surface, which is converted to ZnO in the subsequent heat treatment. The tracer used was Zn-65. After 50 hr at 400°C, the oxide was removed in 4 to 5 layers by etching in dilute acetic acid. Uniformity of removal was checked by reversal of the interference colors of the oxide. Nevertheless, the etching procedure is a source of major error in the experiments, which, therefore, have only a semiquantitative value.

In Fig. 4 is a plot of the activity of Zn as a function of distance in the oxide layer. From this curve the diffusion coefficient of Zn in the ZnO film can be estimated to be $D = 10^{-16}$ cm^2sec^{-1}. The parabolic rate constant at 400°C is $k = 1.8 \times 10^{-16}$ cm^2sec^{-1}. This result is good evidence against the mechanisms of oxygen diffusion (*a*, *b*) which would predict

virtually no diffusion of the Zn through the oxide. It also tends to disprove the surface reaction mechanism (*e*), which would predict extremely rapid diffusion of zinc, and an almost uniform distribution of Zn* through the oxide layer.

The large negative ΔS^* for the oxidations of zinc and aluminum remains difficult to explain, and further experimental work on these reactions is obviously required.

Linear Rate Constants

Relatively few measurements of the linear rate constants are available, but this subject should be one of increasing interest in view of the fundamental importance of the elementary reactions involved. The available data are summarized in Table IV. The rate constants k_0 are expressed in the form $k_0 = A \exp(-E/RT)$, with A in gram atoms of oxygen per cm² sec. The constants appear to fall into two groups, those with small A and large E, and those with large A and small E.

TABLE IV. *Linear rate constants* $k_0 = A\, e^{-E/RT}$ *for metal oxidation*

Metal	Temp range	A	E	Reference
	°C	*eq cm⁻²sec⁻¹*	*kcal*	
Ca	300–500	6.6×10^{-6}	8.1	(60)
Th	350–500	5.2×10^{-2}	22.0	(61)
Ta	300–500	1.0×10^{-5}	20.8	(5)
Ti	650–930	2.8	43.8	(4)
Al	400–550	6.5×10^{5}	47.7	(47)
Mg	410–575	1.1×10^{9}	50.5	(3)

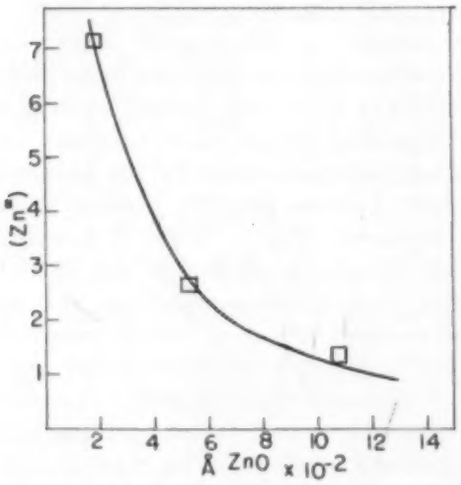

FIG. 4. Diffusion of radioactive Zn in ZnO film on zinc foil. Distribution of Zn after 40 hr at 400°C.

If an over-all reaction proceeds through two consecutive steps, e.g., metal oxidation proceeding through diffusion followed by interface reaction, the step with the smaller activation energy will tend to become rate-determining at the higher temperatures. The linear rate constants for titanium, aluminum, and magnesium, as given in Table IV, have higher activation energies than the parabolic constants for the same metals. It may be concluded that these linear rates are not steps in the low temperature, diffusion controlled oxidation. They probably represent reactions at a metal to oxygen interface, and not at an oxide-oxygen or oxide-metal interface.

In the cases of calcium, thorium, and tantalum, on the other hand, the linear rates may well be reactions at the oxide-oxygen interface, i.e., steps in a sequence of diffusion and interface reaction. It would probably be premature to attempt any more detailed analysis of the linear rates at this time.

Acknowledgments

The author is indebted to the John Simon Guggenheim Memorial Foundation and to the United States Educational Commission in the United Kingdom for the award of fellowships under which much of this work was carried out at the H. H. Wills Physical Laboratory of the University of Bristol. Special thanks are due to Professor N. F. Mott, Dr. J. Friedel, and Dr. A. Seeger for interesting and helpful discussions.

Any discussion of this paper will appear in a Discussion Section, to be published in the June 1954 issue of the JOURNAL.

REFERENCES

1. C. WAGNER, *Z. physik. Chem.*, **21B**, 25 (1933).
2. C. WAGNER AND W. SCHOTTKY, *Z. physik. Chem.*, 11B, 163 (1930).
3. T. E. LEONTIS AND F. N. RHINES, *Trans. Am. Inst. Mining Met. Engrs.*, **166**, 265 (1946).
4. M. H. DAVIES AND C. E. BIRCHENALL, *J. Metals*, **3**, 889 (1951).
5. J. K. LEE, Dissertation, Catholic University, Washington, D. C. (1952).
6. K. HAUFFE AND H. PFEIFFER, Vorberichte zur Diskussions u. Sondertagung, p. 206, Deutsche Bunsen Ges., Berlin (1952).
7. F. BOOTH, *Trans. Faraday Soc.*, **44**, 796 (1948).
8. H. S. CARSLAW AND J. C. JAEGER, "Conduction of Heat in Solids," p. 105, Oxford University Press, Oxford England (1947).
9. N. F. MOTT AND R. W. GURNEY, "Electronic Processes in Ionic Solids," p. 257, Oxford University Press, Oxford, England (1940).
10. N. CABRERA AND N. F. MOTT, *Repts. Prog. Phys.*, **12**, 163 (1949).
11. C. A. HOGARTH, *Z. physik. Chem.*, **198**, 30 (1951).
12. E. E. HAHN, *J. Appl. Phys.*, **22**, 856 (1951).
13. J. A. KITCHENER AND S. IGNATOWICZ, *Trans. Faraday Soc.*, **47**, 1278 (1951).
14. J. FRIEDEL, Private communication (1951).
15. P. H. MILLER, *Phys. Rev.*, **60**, 890 (1941).
16. N. F. MOTT AND R. W. GURNEY, "Electronic Processes in Ionic Crystals," p. 158, Oxford University Press, Oxford, England (1940).
17. F. C. FRANK, *Phil. Mag.*, (7), **41**, 1287 (1950).

18. D. J. M. Bevan, J. P. Shelton, and J. S. Anderson, *J. Chem. Soc.*, **1948**, 1729.
19. D. J. M. Bevan and J. S. Anderson, *Disc. Faraday Soc.*, **8**, 238 (1950).
20. E. S. Rittner, R. A. Hutner, and F. K. Dupre, *J. Chem. Phys.*, **17**, 198 (1949); **18**, 379 (1950).
21. N. F. Mott and M. J. Littleton, *Trans. Faraday Soc.*, **34**, 485 (1938).
22. U. Croatto and R. Mayer, *Gazetta chim. ital.*, **73**, 199 (1943).
23. J. S. Anderson, *Proc. Roy. Soc.* (A), **215**, 353 (1952).
24. C. Wagner and E. Hammen, *Z. physik. Chem.*, **40B**, 197 (1938).
25. M. J. Bénard, *J. chim. phys.*, **44**, 266 (1947).
26. L. S. Darken and R. W. Gurry, *J. Am. Chem. Soc.*, **67**, 1407 (1945).
27. J. H. DeBoer and E. J. W. Verwey, *Proc. Phys. Soc.*, **49**, extra part, 59 (1937).
28. H. M. O'Bryan and H. W. B. Skinner, *Proc. Roy. Soc.*, **A176**, 229 (1940).
29. N. F. Mott and R. W. Gurney, "Electronic Processes in Ionic Crystals," p. 75, Oxford University Press, Oxford, England (1940).
30. R. W. Wright and J. P. Andrews, *Proc. Phys. Soc.*, **A62**, 446 (1949).
31. H. B. Michaelson, *J. Franklin Inst.*, **249**, 472 (1950).
32. J. Bardeen and C. Herring, "Imperfections in Nearly Perfect Crystals," Chapter X, John Wiley and Sons, Inc., New York (1952).
33. H. Eyring, *J. Chem. Phys.*, **4**, 283 (1936).
34. C. Zener, *J. Appl. Phys.*, **22**, 74 (1951).
35. G. J. Dienes, *Phys. Rev.*, **89**, 185 (1953).
36. J. C. Fisher, *J. Appl. Phys.*, **22**, 74 (1951).
37. W. J. Moore and B. Selikson, *J. Chem. Phys.*, **19**, 1539 (1951).
38. R. Lindner, *Acta Chem. Scand.*, **6**, 457 (1952).
39. G. Valensi, *Proc. Pittsburgh Intl. Conf. Surface Reactions*, p. 156 (1948).
40. W. J. Moore and J. K. Lee, *Trans. Faraday Soc.*, **48**, 916 (1952).
41. O. Kubaschewski and O. Goldbeck, *Z. f. Metallkunde*, **39**, 158 (1948).
42. W. J. Moore and J. K. Lee, *J. Chem. Phys.*, **19**, 255 (1951).
43. M. H. Davies, M. T. Simnad, and C. E. Birchenall, *J. Metals*, **3**, 889 (1951).
44. E. A. Gulbransen, *Ind. Eng. Chem.*, **41**, 1385 (1949).
45. E. A. Gulbransen and K. F. Andrew, *J. Electrochem. Soc.*, **97**, 396 (1950).
46. W. J. Moore and J. K. Lee, *Trans. Faraday Soc.*, **47**, 501 (1951).
47. E. A. Gulbransen and W. S. Wysong, *J. Phys. Chem.*, **51**, 1087 (1947).
48. E. A. Gulbransen and K. F. Andrew, *J. Metals*, **185**, 741 (1949).
49. E. A. Gulbransen and K. F. Andrew, *J. Metals*, **185**, 515 (1949).
50. D. Cubicciotti, *J. Am. Chem. Soc.*, **72**, 2084, 4138 (1950).
51. E. A. Gulbransen and K. F. Andrew, *J. Electrochem. Soc.*, **97**, 383 (1950).
52. E. A. Gulbransen and K. F. Andrew, *J. Electrochem. Soc.*, **99**, 402 (1952).
53. E. A. Gulbransen and K. F. Andrew, *J. Metals*, **188**, 586 (1950).
54. W. H. J. Vernon, E. I. Akeroyd, and E. G. Stroud, *J. Inst. Metals*, **65**, 301 (1939).
55. C. Wagner and K. Gruenwald, *Z. physik. chem.*, **40B**, 455 (1938).
56. H. J. Engell and K. Hauffe, *Metall*, **6**, 285 (1952).
57. W. J. Moore, *Phil. Mag.*, (7), **43**, 688 (1952).
58. J. Bardeen, W. H. Brattain, and W. Shockley, *J. Chem. Phys.*, **14**, 714 (1946).
59. G. W. Castellan and W. J. Moore, *J. Chem. Phys.*, **17**, 41 (1949).
60. R. E. Pilling and N. Bedworth, *J. Inst. Metals*, **29**, 534 (1923).
61. P. Levesque and D. Cubicciotti, *J. Am. Chem. Soc.*, **73**, 2028 (1951).

Surface Reactions of Steel in Dilute $Cr^{51}O_4^=$ Solutions: Applications to Passivity[1]

R. A. Powers[2] and Norman Hackerman

Department of Chemistry, University of Texas, Austin, Texas

ABSTRACT

Interactions between a steel surface and anions containing chromium-VI were studied by radiotracer methods supplemented by contact potential measurements. In chromate solutions of high enough concentration, the behavior of steel is analogous to that of chromium, i.e., it is passive and is found to remove a definite number of chromate ions from solution. The relationships among solution composition, radioactivity retained on the passive surface, and contact potential indicate that at least a portion of the activity is present as adsorbed chromate ion. In dilute solutions, where corrosion occurs, radioactive chromium in excess of that associated with a passive surface appears on both anodic and cathodic areas.

Deductions relative to the structure of a passive surface are made from these and other data from the chromium-chromate system.

Introduction

An earlier paper (1) gives the results of an investigation of the type and extent of interaction between a chromium surface and chromate ion in solution. In order to have the comparison between a naturally passive and a naturally active metal, many of the experiments performed with the chromium-chromate system were repeated using steel surfaces. The object of this paper is to present these data together with some deductions relative to the structure of passive surfaces.

Other work with radioactive chromate and steel surfaces has been reported (2, 3), but these have been of a preliminary nature with few or no experimental details.

Experimental

The general experimental approach was similar to that described for the chromium-chromate system (1), and consisted of counting the radioactivity retained on a steel surface after contact with an aqueous solution of radioactive chromium-VI anions of given concentration and *p*H. Supplementary data were obtained from changes in contact potential of coupons immersed in inactive solutions of identical concentration and *p*H. Contact potentials were measured vs. abraded and aged platinum by the method of Zisman (4).

Reacting surfaces were prepared from S.A.E. 1020 steel. Disks 2.8 cm in diameter by 0.8 mm thick were used for contact potential measurements, and 3 cm x 6 cm sheets of the same thickness were formed into hemicylinders for immersion in most of the radioactive solutions. This shape was used in order to obtain optimum geometric relationship between counter tube and sample. In the initial experiments where autoradiographs were taken, flat samples were used. Coupon surfaces were abraded just before use with No. 2 emery, scrubbed with thiophene-free benzene and allowed to air dry. This treatment produced a surface (at least partially oxidized) giving satisfactorily reproducible results ($\pm 10\%$).

The roughness factor of the steel surfaces used was not known with the same accuracy as were the counting and contact potential data. Use of a modification (5) of the polarization capacity method of Wagner (6) gave an average value of 20 for the coupons themselves. The roughness factor for Armco iron abraded with No. 2 emery was found by krypton adsorption at liquid nitrogen temperatures to be 3.8. In view of the meager data in the literature for the roughness factor of analogous surfaces, it is at present impossible to assign a very definite value to the roughness factor.

Radioactive solutions were prepared by dilution of a stock sodium chromate solution made with double distilled water. The sodium chromate was obtained by oxidation of spectroscopically pure chromium which had been partially converted to Cr^{51} (1). The systems were open to air.

Results

Effect of Concentration; Passivating vs. Corrosive Solutions

Initial experiments consisted in immersing flat abraded steel plates (2.5 cm x 7.5 cm x 1.55 mm) in

[1] Manuscript received March 29, 1952. This paper was prepared in part for the Detroit Meeting, October 9 to 12, 1951.

[2] Magnolia Petroleum Company Fellow in Physical Chemistry, 1950–51. Present address: National Carbon Research Laboratories, Box 6087, Cleveland, Ohio.

active chromate solutions in the range of 10^{-4} to $10^{-3}M$ and at *p*H 7.5. This range was dictated by the amount of active chromate available and by the fact that $10^{-3}M$ chromate passivates steel while $10^{-4}M$ does not. The coupons were exposed to 200 ml of solution for 48 hours, at the end of which time three distinct and reproducible behavior patterns appeared:

1. Coupon 1 ($10^{-4}M$ solution), active corrosion with large anodic and cathodic areas. The corrosion products were easily removed by simple wiping and showed a high concentration of radioactive chromium. There was no radioactivity on the anodic areas after removal of the loose corrosion products, but the bright cathodic areas were highly active (see Table I and Fig. 1a). The radioactivity from the cathodic areas could not be removed either by wiping or by scrubbing with filter paper or cloth.

2. Coupon 2 ($3 \times 10^{-4}M$ solution), most of the coupon remained bright and uncorroded but a few small anodic areas appeared bearing an adherent corrosion product which could not be removed by washing or wiping. The data of Table I and Fig. 1b show that the areas of corrosion product bear some excess radioactivity, but that most of that on the coupon as a whole is distributed over the uncorroded surfaces.

3. Coupons 3 and 4 (7×10^{-4} and $10^{-3}M$ solution), remained perfectly bright and free of any visible corrosion product, i.e., were passivated by the chromate solutions. The counting data and autoradiographs (Table I and Fig. 1c) show that within the resolving power of the radiographs in each case a definite and uniformly distributed amount of radioactive chromium was retained on the steel surfaces. This activity could not be removed by any nondestructive physical treatment of the surface such as rubbing, washing, or boiling in distilled water.

Additional information was obtained by returning coupons 3 and 4 to their respective solutions for an additional period of 72 hours. In all instances, coupon 4 remained passive, showing no change either in appearance or in acquired radioactivity. However, coupon 3 in $7 \times 10^{-4}M$ solution tended to become badly corroded and picked up additional activity both in the corrosion product and on the cathodic (uncorroded) areas.

The inferences from these data are quite plain. In the case of complete passivation (coupon 4 in $1 \times 10^{-3}M$ chromate), a definite amount of uniformly distributed radioactivity appears on the passive steel surface, and is indeed a discrete portion of that surface since it cannot be removed by simple physical means. Where slight attack occurs in the presence of chromate ion (coupon 2 in $3 \times 10^{-4}M$ solution), the pickup of radioactivity increases some-

TABLE I. *Radioactivity picked up by steel surfaces*

Chromate conc.	Coupon	c/m	Remarks
$1 \times 10^{-4}M$	1	377	Extensive corrosion after 24 hours. Distinct anodic and cathodic areas. Corrosion products nonadherent and removed before counting. (Fig. 1a).
$3 \times 10^{-4}M$	2	175	Few small areas of corrosion. Corrosion product very adherent and not removed. (Fig. 1b).
$7 \times 10^{-4}M$	3	153	No visible corrosion.
$1 \times 10^{-3}M$	4	151	No visible corrosion. (Fig. 1c).

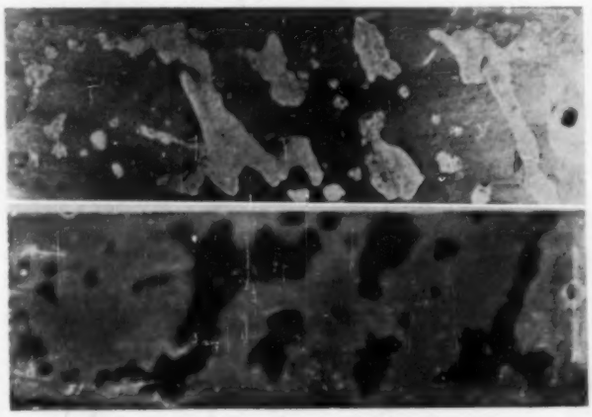

FIG. 1a. A corroded steel coupon after exposure to $1 \times 10^{-4}M$ chromate (upper) and its radioautograph. Dark portions of latter are anodic areas on which no Cr^{51} was retained. (Corrosion products removed from anodic areas before radioautographs prepared.)

FIG. 1b. Radioautograph of steel coupon showing high concentration of radioactivity at circled spots. These spots are caused by adherent corrosion products. Exposure was to $3 \times 10^{-4}M$ chromate.

FIG. 1c. Radioautograph of passive steel coupon showing apparent uniform distribution of Cr^{51}. Exposure was to $1 \times 10^{-3}M$ chromate.

what and at least a portion of the extra chromium is associated with the points of corrosion, almost certainly with the adhering corrosion product. In the case of intense corrosion resulting in a voluminous, loose corrosion product, the activity picked up by the steel rises sharply, and the increase is found to be associated not only with the corrosion products but also with the cathodic portions of the surface.

Considering now only the case of a steel surface passivated in 1 x $10^{-3}M$ chromate solution of *p*H 7.5, it was shown that a fixed and reproducible amount of Cr^{51} activity was associated with the passive surface. In terms of chromate ion this radioactivity represents 5.2 x 10^{15} ions per cm^2 of projected area, or 48 x 10^{-8} grams of chromium per cm^2. Hoar and Evans (7) have reported 3.4 x 10^{-8} g/cm^2 of chromium in films stripped from steel passivated in 0.67M chromate. Brasher and Stove (2) report 5.5 x 10^{15} chromate ions per cm^2 are taken up from 0.1 per cent radioactive potassium chromate solution of unspecified *p*H.

TABLE II. *p*H *changes produced by steel in chromate solution*

Initial *p*H	Δ*p*H
4.2	+0.1
6.0	+0.1
7.8	−0.2
9.25	−1.2
10.3	−0.4
11.15	±0.0

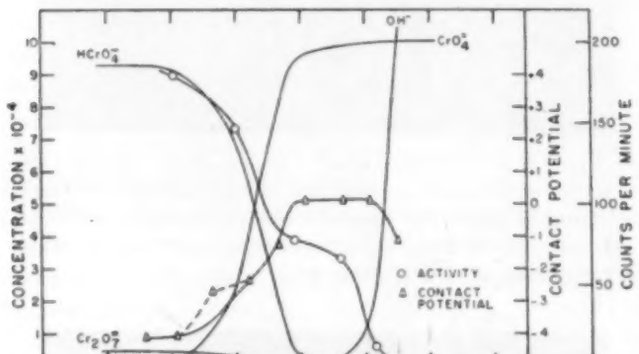

FIG. 2. Relationships among ionic species in solution, *p*H, activity pickup, and contact potential for steel-chromate system.

Effect of *p*H *on the Activity Retained by Passive Surfaces*

The data presented in the foregoing section established the fact that at *p*H 7.5 a steel surface passivated by chromate solution retains a fixed and reproducible amount of chromium in one form or another. In the previous work (1) with passive chromium surfaces in radioactive chromate solutions, a quantitative relationship was found between solution *p*H and the amount of activity retained by the chromium surface. It was of interest, therefore, to determine if passive steel surfaces exhibited an analogous behavior.

It must be emphasized that, in all experimental procedures which follow, passive, or at least visibly uncorroded, surfaces were dealt with and that at no time was it possible to detect differences among the exposed coupons other than by differences in radioactivity and contact potential.

Solutions originally 1 x $10^{-3}M$ in chromate ion and covering the *p*H range of 11.1 to 4.2 were prepared as described elsewhere (1). Two sets of initial determinations were made. In the first, the coupons were exposed to the active solutions for 72 hours; in the second, for 120 hours. At the end of these periods coupons were removed, rinsed in distilled water to remove physically adhering solution, blotted dry with filter paper, and counted. Later experimentation showed that the same results could be obtained with one-hour exposures, i.e., the equilibration period of the system did not exceed one hour.

The 72-hour counting data as a function of initial solution *p*H are plotted as circles in Fig. 2. The overall relationship between activity retained by the passive steel surface and solution *p*H is identical to that found for chromium in more dilute solutions. Moreover, there was a marked change in *p*H of the solutions during equilibration just as there was with the chromium-chromate system. These changes are given in Table II and are similar to those for the chromium-chromate system (1).

A point of particular interest is that coupons in the active solutions of *p*H 11.0 acquired absolutely no radioactivity from solution although they were no different in appearance from the rest.

In an effort to identify the form in which chromium was retained on or by the steel surface, exchange experiments were tried using inactive solutions of sodium chromate and chromium-III nitrate. In neither case was exchange of the surface radioactivity observed in either hot or cold solutions.

Contact Potentials of Passive Steel Surfaces; Effect of *p*H

Contact potential data were obtained by exposing steel disks to 1 x $10^{-3}M$ nonradioactive chromate solutions covering the *p*H range of 3.3 to 11.0. All potentials reported are vs. abraded and aged platinum as reference. Positive values indicate a decreasing electronic work function relative to platinum, and negative values an increasing work function. The contact potential of any given steel coupon was found to rise slowly upon removal from chromate

solution and exposure to the air, and data were obtained by removing only one coupon at a time from solution and measuring its potential within 30 seconds after washing in distilled water and blotting dry.

The contact potential of the original abraded disks was found to be uniformly +0.4 volt in agreement with the value reported by Uhlig (8). Immersion of these disks in inactive solutions of chromium-VI anions over the *p*H range of 3.3 to 11.0 produced changes from the initial +0.4 volt to the values shown in Fig. 2. The particular data shown are for 24-hour exposure to the solutions. Shorter periods of contact (such as one hour) resulted in curves of identical form but displaced to somewhat lower values (0.05 to 0.1 volt). Coupons exposed to sodium hydroxide of *p*H 11.0 exhibited essentially the same final potential as those in chromate solution of the same *p*H. For example, Fig. 2 shows steel exposed to 1 x $10^{-3}M$ chromate solution of *p*H 11.0 to have a contact potential of −0.12 volt and to have picked up no radioactivity from solution. The contact potential of a similar coupon in 1 x $10^{-3}M$ sodium hydroxide (*p*H 11.0) was found to be −0.15 volt.

It should be noted that the entire contact potential curve of Fig. 2 lies at least 0.4 volt below the potential of the original abraded surface. At each point the contact potential (ΔV) of a surface is given by:

$$\Delta V = 4\pi\mu\eta$$

where μ is the dipole moment per unit area, and η is the number of molecules per unit area. Thus, one important consequence of the contact potential data is that the passivation of a steel surface by chromate or dichromate of any *p*H results in a considerable change in its net dipole moment. The direction of change is such that it represents a dipole oriented with its negative end toward the solution side of the interface and its positive end toward the metal. The second consequence is that the net change observed is a sensitive function of solution *p*H just as was the amount of radioactivity retained on the surface.

Discussion

Interpretation of Results

Fig. 2 as a whole represents the effect of solution *p*H as the independent variable on three separate dependent quantities: the radioactivity retained on a steel surface in equilibrium with an active solution of chromium-VI anions, of given *p*H; the contact potential of that surface; and the concentration of the various anionic species present. Inspection of this figure shows that there is almost certainly a relationship between the composition of the solution, the radioactivity acquired, and contact potential. In fact, solution composition rather than *p*H may be regarded as the true independent variable. For example, at *p*H 8.0 and below, the solution changes composition from essentially pure chromate to a mixture of hydrogen chromate and dichromate, and at exactly the same *p*H the activity and contact potential curves undergo a rapid change in slope. In a like manner those portions of the curves between *p*H 11.0 and 8.0 represent a region of constant chromate concentration but an exponentially decreasing hydroxyl ion concentration. Thus, one must conclude that the observed properties of passive steel surfaces given in Fig. 2 are a function of the environment to which they were exposed, i.e., the type and number of anions in solution. In this respect there is complete agreement with the analogous passive chromium-chromate system for which similar contact potential, radiotracer, and *p*H data have been found (1).

In a previous section it was shown that one of the steel surfaces passivated at *p*H 7.5 in 1 x $10^{-3}M$ chromate solution retained 48 x 10^{-8} grams of chromium/cm², or the equivalent of 5.2 x 10^{15} chromate ions. Considering this number of ions close packed on the surface with a roughness factor of either 20 or 4, one calculates the equivalent of 0.65 or 3.25 monolayers of chromate ion.

The question naturally arises as to the chemical and physical form of the chromium which has been shown to be firmly fixed in or on a steel surface passivated in chromate solution. In forming conclusions, the following experimental and derived facts were considered:

1. The amount of radioactive chromium retained by a passive steel surface in the solutions employed is a definite and reproducible function of the type and concentration of the anionic species in solution, and through this mechanism a function of solution *p*H.

2. The contact potentials of passivated steels are related to solution *p*H and composition and/or the amount of chromate ion removed from solution. In other words, the average dipole moment of a passive steel surface is a function of the type and relative numbers of anions in the solution producing it.

3. A steel coupon passivated in 1 x $10^{-3}M$ chromate solution of *p*H 11.0 acquires no radioactivity and exhibits the same contact potential as if in sodium hydroxide alone of the same *p*H. This permits the conclusion that hydroxyl ion rather than chromate ion has determined the passive character of the surface in this instance.

4. Over the *p*H range of 11.0 to 8.0 there exists an inverse relationship between the number of chromate ions removed from solution by steel and the change in hydroxyl ion concentration as indicated by *p*H. In addition it may be shown from Fig. 2 that the activity vs. *p*H curve above *p*H 8.0 is a function of the chromate to hydroxyl ratio.

5. The radioactivity on a passive steel surface is firmly fixed, and does not exchange with either chromium-III or chromium-VI in solution.

6. Roughness factor and counting data indicate a maximum of 3.25 equivalent monolayers of chromate ion removed from solution of *p*H 8.0 and 1 x $10^{-3}M$ in concentration. This may be less if the total area seen by the ions in solution is more closely given by the polarization capacity, a solution method, than by gas adsorption. This is clearly a debatable point which can be settled only by much more extensive work on available 'real' area.

7. The data of Fig. 2 and the facts outlined above are analogous to those of the passive chromium-chromate system where anion exchange properties have been demonstrated (1).

It is concluded that the best interpretation of all of these facts is that these passive steel surfaces must have as their outermost component an equivalent monolayer of irreversibly adsorbed anions. Without this concept it is not possible to explain the dependence of both counting and contact potential data on solution composition, or the relationship between chromate or dichromate ion removed from solution and contact potential. If only the counting and roughness factor data are considered, a decision as to the nature of the surface is more difficult. For example, the activity vs. *p*H curve of Fig. 2 could be interpreted as representing reduction to chromium-III which was then retained on the surface. However, the contact potential data represent changes in dipole moment which cannot be related to a change in extent of a single reaction such as chromium-VI reduction. If such were the case, then the contact potential vs. *p*H curve should bear a constant relationship to the activity vs. *p*H data, which it does not. At *p*H 7.5 and below, for example, the activity and contact potential curves diverge sharply.

The data of Fig. 2 represent, therefore, an indication of the type and relative numbers of the various anions held by the passive steel surface. Between *p*H 11.0 and 8.0 the data represent simply the ratio of chromate ion to hydroxyl ion in the adsorbed layer and this in turn is a reflection of their ratio in solution. At *p*H 11.0, where both ions are of equal concentration in solution, only hydroxyl is adsorbed. At *p*H 8.0 chromate ion is essentially the only anion present, and hence makes up the monolayer. Below *p*H 8.0 the solutions become increasingly poorer in chromate ion and more concentrated in dichromate and hydrogen chromate. Since the activity retained continues to increase over this region, the indication is that chromate ion is continually displaced by dichromate (or polylayer hydrogen chromate) as the concentration ratio changes. In this connection it is of interest to note that the count at *p*H 3.3 is twice that at *p*H 8.0.

In the absence of more conclusive surface area data, it is not possible to say that adsorption is the only process whereby chromate or other anions may become a firm portion of a passive steel surface. For example, work with chromium (1) suggests that an oxide layer rather than the metal itself is the adsorbent for chromate and other anions. In the case of the steel surfaces used, we know them to bear some abrasion-produced oxide layer. It may be that some of the chromate removed from solution goes into the completion of this layer and explains the greater than monolayer coverage. This, however, does not detract from the main argument that at least one equivalent chemisorbed monolayer of chromate or other anion must constitute the outermost surface of passive steel.

Applications to Passivity; Passive vs. Active Metals

Where conditions were such as to induce passivity, the behavior of steel in chromate solutions was analogous to that of chromium. A definite and reproducible amount of radioactivity on the surface was found to be associated with the passive state. The effect of *p*H on activity picked up and on contact potential was found to be the same as that observed for chromium and is explainable on the same basis, i.e., preferential adsorption of a given anion.

The principal difference between the two metals is that chromium was passive in all solutions employed, while steel required a definite and fairly high chromate concentration for passivity. Chromium exhibited a greater affinity for chromate than did steel, since it acquired maximum activity from 5 x $10^{-6}M$ solutions, while steel required a concentration of 1 x $10^{-3}M$ or higher. However, the equilibrium period for steel was only one hour compared to 14 days for chromium.

These data suggest that chromium has a surface with a high tendency to chemically adsorb environmental constituents. This tendency is so great that chromium seldom exists without such a layer, so that replacement of one species by another is a lengthy process. Steel, on the other hand, adsorbs a more select group of species under more stringent conditions, but since abraded steel does not have associated with it any firmly sorbed species, pickup of chromate or other ion should be rapid. In other

words, the behavior of chromium is indicative of exchange adsorption, whereas that of abraded steel represents primary adsorption. In either case the end point is the same.

The principal argument up to this point has been that there is associated with a passive steel or chromium surface a definite number of adsorbed anions. The fundamental differences in behavior between steel and chromium which have been outlined above further suggest that this adsorbed layer is an integral part of the passive state rather than a reproducible coincidence. As supporting evidence, consider the instance of chromium in mixed solution of chromate and sulfate or chloride ions (1), where, under adverse ionic ratios, chromate ion is adsorbed as strongly as if present alone, i.e., there is a greater tendency for a passivating anion to appear in the adsorbed layer than a neutral or nonpassivating one. One may, therefore, conclude that the adsorbed layer is itself partially responsible for passivity.

Data from the steel-chromate system add weight to the belief, advanced earlier (1), that a passive surface consists of an oxide layer bearing adsorbed anions of a specific type. In addition to the fact that the postulate of competitive adsorption best explains the experimental data, it is known that the steel surfaces used bore an abrasion-produced oxide which was nonprotective in the absence of specific anions.

The behavior of steel surfaces in chromate solutions of *p*H 11 and above is of particular interest. These surfaces were passive, yet picked up no radioactivity from solution. Passivity under these conditions must be attributed to the presence of hydroxyl ions, and is offered as additional evidence that passivity may be induced by nonoxidizing anions. Robertson (9) has shown that molybdate and tungstate ions in concentrations above $10^{-3}M$ passivate iron, and are comparable to chromate in their action. However, these ions are poorer oxidizing agents than chromate, so that their action may be attributed to adsorption.

The interpretation of a passive surface based on the evidence given here is somewhat similar to that of Hoar and Evans (10) in their revised theory of passivity and inhibition. These authors postulate that the protective value of an oxide is related to the ability of metal ions to migrate through it. A nonprotective oxide is one which is deficient in cations so that ions from the basis metal may migrate from defect to defect until they reach the surface. A corrosion inhibitor or passivator then becomes any environmental constituent which reacts with metal ions at the interface to produce an insoluble product. An accelerator is any ionic or molecular species which forms a soluble product or complex with the metal ions and leaves the way open for further migration. The data presented here, however, indicate that adsorbed anions at the oxide-solution interface rather than reaction products can be responsible for passivity.

Acknowledgment

The authors are grateful for the financial support given this work by the Office of Naval Research under Contract N5ori-136 T.O. II.

Any discussion of this paper will appear in a Discussion Section, to be published in the June 1954 issue of the Journal.

REFERENCES

1. N. Hackerman and R. A. Powers, *J. Phys. Chem.*, **57**, 139 (1953).
2. D. M. Brasher and E. R. Stove, *Chemistry & Industry*, **8**, 171 (1952).
3. M. T. Simnad, *J. Metals*, **188**, 1220 (1950).
4. W. A. Zisman, *Rev. Sci. Instr.*, **3**, 267 (1932).
5. B. Pegues, "Polarization Capacity and the Roughness of Metal Surfaces," M.A. Thesis, University of Texas, Austin, Texas (1951).
6. C. Wagner, *J. Electrochem. Soc.*, **97**, 71 (1950).
7. T. P. Hoar and U. R. Evans, *J. Chem. Soc.*, **1932**, 2476.
8. H. H. Uhlig, *J. Appl. Phys.*, **22**, 1399 (1951).
9. W. D. Robertson, *J. Electrochem. Soc.*, **98**, 94 (1951).
10. T. P. Hoar and U. R. Evans, *J. Electrochem. Soc.*, **99**, 212 (1952).

Quinones as Ion Source in Hydrocarbons[1]

ANDREW GEMANT

Engineering Laboratory and Research Department, The Detroit Edison Company, Detroit, Michigan

ABSTRACT

When orthodihydric phenol solutions in hydrocarbons or dioxane are subjected to oxidation, marked increase in electric conductivity takes place. Various aspects of this observation were studied experimentally, such as: the effect of the time of oxidation; effect of dilution; decay with time of the conductivity; d-c polarization; role of quinone concentration; effect of temperature of oxidation. The experimental results are tentatively explained by a generation during oxidation of intermediate ionic stages of relatively high stability. These oxidative ions, both positive and negative, might be semiquinones having completed electronic shells. Ions of this type appear to be representative of ions formed during oxidation of dielectric liquids.

INTRODUCTION

The purpose of this study was to obtain information on the chemical nature of ions present in oxidized hydrocarbons. In a previous paper (1) the author reported on studies of oxidized aldehyde solutions in hydrocarbons. Those results indicated that, on oxidation, orthodihydric phenols produced conductivities in some ways similar to those found in oxidized oils. It was concluded that ions derivable from such compounds are, to a certain degree, representative of ions in oxidized hydrocarbons. In the present paper a description of experimental results with dihydric phenols, mentioned only briefly in the paper cited, is presented in greater detail. In addition, the possible mechanism of ion formation, as well as their possible chemical structure, is presented.

CONDUCTIVITY OF OXIDIZED CATECHOLS

It was found that, upon oxidation, a solution of a dihydric phenol in a hydrocarbon showed a marked increase in electrical conductivity. The phenols used in these experiments were pyrocatechol and *p*-tert-butylcatechol; the latter was purified by distillation of the Eastman product. The hydrocarbons used were benzene, xylene, 2-2-4 trimethylpentane, *n*-octane, *n*-heptane, a hydrocarbon oil (viscosity 0.14 poise at 25°C) and, in addition, *p*-dioxane. The following oxidizing agents were used: potassium permanganate, potassium dichromate, magnesium perchlorate, silver oxide, sodium perborate, barium peroxide, and ozone. In all hydrocarbons, butylcatechol was used because of its high solubility; pyrocatechol was used with dioxane as solvent. The various combinations of solvents and oxidizing agents gave conductivity effects greatly varying in magnitude; in certain cases there was no effect observable. The experiments were carried out in stoppered graduated cylinders containing the solution and the oxidizing solid, and shaken at intervals.

Typical results are presented in Fig. 1 for benzene as solvent. All conductivities were obtained from bridge measurements using 100 to 1000 cps. The graphs show conductivity as a function of oxidation time for four solid oxidants. The concentration of butylcatechol was 3 millimole per liter. The effect is rather pronounced, the increase apparently continuing beyond the duration of the experiment for $KMnO_4$ and Ag_2O, the two strongest oxidants. In the majority of the combinations a yellow coloration appeared, increasing in intensity with time, as a sign that part of the catechol was converted to *o*-quinone. This point is discussed in greater detail later. On repeating experiments of this kind, the qualitative effect always remains the same, but the magnitude of the conductivities attained may in some cases show appreciable variation.

Fig. 2 presents results on hydrocarbon oil. Curve 1 shows that the effect is again rather pronounced; so was the yellow coloration. The yellow-reddish color of oxidized oils may be due partly to the quinone type of compounds. A control test was carried out with an addition of anhydrous Na_2SO_4 to check whether water formed during oxidation played a role in the conductivity effect; it may be seen that this is not the case. Curve 3 refers to a control test with $KMnO_4$ but without butylcatechol; it may be seen that oxidation of the latter is, indeed, the cause of the effect.

Fig. 3 refers to similar tests on two octanes with a dichromate and a peroxide as oxidants. It may be added that with permanganate the increase in conductivity in octanes was markedly greater.

Fig. 4 presents results with pyrocatechol and dioxane as solvent. The effect is particularly pronounced with silver oxide as oxidant. It may be re-

[1] Manuscript received November 21, 1952. This paper was prepared for delivery before the New York Meeting, April 12 to 16, 1953.

called that, according to Willstätter, silver oxide is the best agent for preparing *o*-quinone from catechol

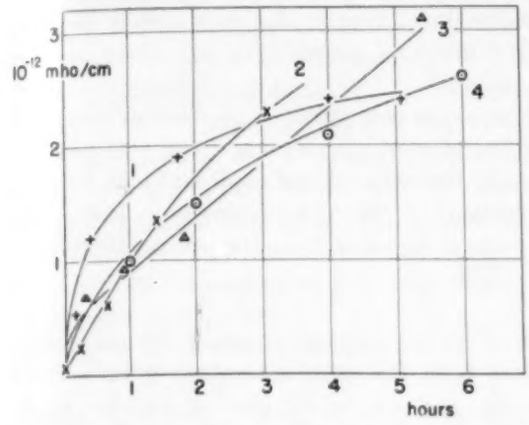

FIG. 1. Conductivity vs. oxidation time for 3 millimole/liter butylcatechol in benzene. Curve 1—$Mg(ClO_4)_2$; curve 2—$KMnO_4$; curve 3—Ag_2O; curve 4—$K_2Cr_2O_7$.

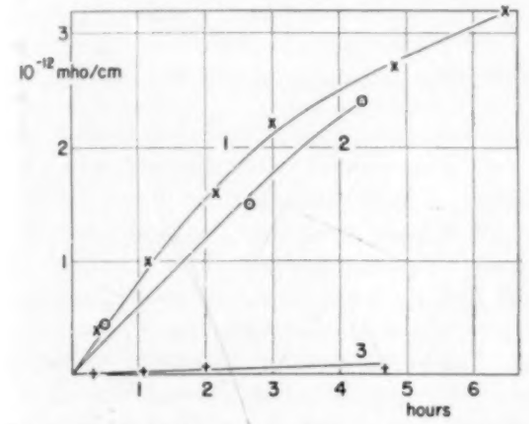

FIG. 2. Conductivity vs. oxidation time for 4.5 millimole/liter butylcatechol in hydrocarbon oil. Curve 1—$KMnO_4$; curve 2—$KMnO_4$ + Na_2SO_4; curve 3—$KMnO_4$ (no catechol).

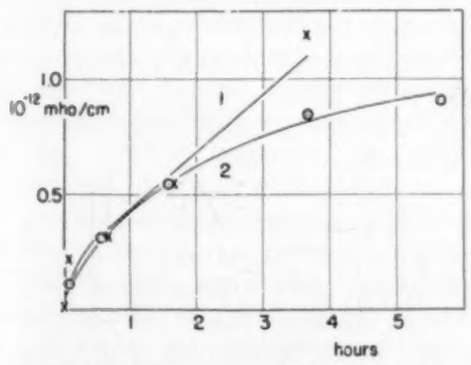

FIG. 3. Conductivity vs. oxidation time for octanes. Curve 1—butylcatechol 3 millimole/liter, trimethylpentane, $K_2Cr_2O_7$; curve 2—butylcatechol 4.5 millimole/liter, *n*-octane, BaO_2.

in ether solutions (2). Curve 3 refers to a control test with Ag_2O, but without catechol.

As mentioned in the author's previous publications, conductivity data are preferably reduced to the same dielectric constant if the variation of the latter in a series of measurements is pronounced. It was ascertained, however, that on oxidizing catechols, this variation is relatively small, and that the effect of the dielectric constant on the conductivity is moderate. The latter is shown for trimethylpentane and dioxane as solvents in Table I, the dielectric constant being increased in steps by additions of small amounts of chloroform. As an example, the total increase of dielectric constant for curve 1, Fig. 3, was 0.012, corresponding to an increase in conductivity of 4 per cent. Similarly, for curve 1, Fig. 4, there is a total increase of dielectric constant of 0.029, corresponding to an increase in conductivity

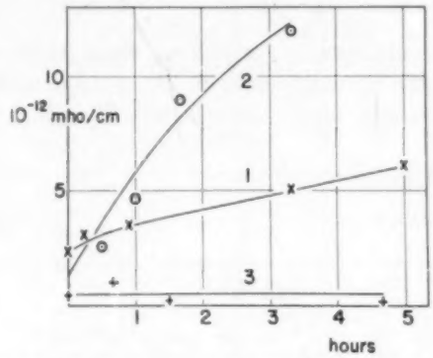

FIG. 4. Conductivity vs. oxidation time for 4 millimole/liter pyrocatechol in *p*-dioxane. Curve 1—$KMnO_4$; curve 2—Ag_2O; curve 3—Ag_2O (no catechol).

TABLE I. *Effect of dielectric constant on conductivity*

Trimethylpentane		*p*-Dioxane	
Dielectric constant	Conductivity	Dielectric constant	Conductivity
	$\times 10^{-12}$ *mho/cm*		$\times 10^{-12}$ *mho/cm*
1.929	13.7	2.370	4.0
1.933	13.8	2.393	4.6
1.942	14.2	2.415	4.9
1.950	14.7	2.435	5.6
1.974	15.9	2.461	6.4
1.999	17.1	2.493	7.4

of 16 per cent. These corrections being relatively small, they were not applied to the data covered by this paper.

A number of check tests were carried out in order to exclude the possibility of incidental causes for the increase in conductivity. In addition to those shown on the previous graphs, a check of *o*-cresol in benzene in contact with $KMnO_4$ may be mentioned. If salt formation were the cause of the effect, substitution of *o*-cresol for catechol should not make a difference since the acid strength of both is about the same. Yet the check test with cresol gave a conductivity of the order of 5×10^{-14}. Water formation also might be a possible cause. When a benzene solution of butylcatechol was kept in contact with water—a

rather severe check—the original conductivity of 1×10^{-13} rose in four hours to about 4×10^{-13}, an order of magnitude about $1/10$ of that shown in Fig. 1. Hence, water formation is not a significant element.

In order to exclude the possibility of metals playing a role in cation formation, ozone was used as oxidizing agent. Ozone was generated in a high-voltage corona ozonizator through which oxygen was passed; this, in turn, was bubbled through the catechol solution in the presence of platinum black as catalyst. The order of magnitude of the flow rate was estimated to one microgram of ozone per second. The increase in conductivity for xylene is shown in Fig. 5. Since platinum black is known to act as a physical catalyst, the test excludes metals as possible cations.

Hydrogen ions are excluded since they exist in measurable amounts only in the presence of strong acids, sulfonic, picric, and the like (3), which are not

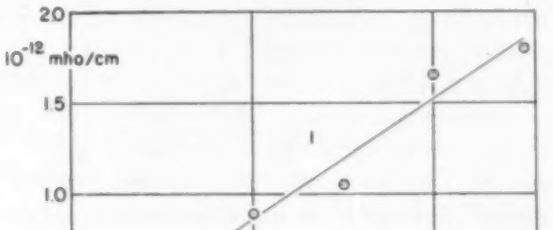

FIG. 5. Conductivity vs. oxidation time for ozone as oxidant in xylene. Curve 1—butylcatechol 6 millimole/liter; curve 2—no butylcatechol.

formed when oxidizing catechols. This was substantiated by standard determination of the acid number of a 3.5 millimole per liter butylcatechol solution in benzene. The acid numbers before and after oxidation with permanganate were 0.015 and 0.020, both very low figures. It follows, therefore, that the cations must be organic ions.

MECHANISM OF ION GENERATION

The question arises, by what mechanism are ions produced during oxidation of catechols? The question has a rather general importance if this type of ion formation is, as assumed, representative of oxidation processes in insulating liquids.

The chief source of ions is the catechol alone, in contrast to conductivities obtainable by the addition of an aliphatic acid, an amine, and a phenol (1), where three components are involved. Catechol is a weak acid (first dissociation constant in water: 3.3×10^{-10}) and is therefore a proton donor and the source of anions. The corresponding proton acceptor, the source of cations, is in all probability an oxidation product; this is the most likely assumption. There are two possibilities for those ions to be generated.

First, one can think of a thermodynamic equilibrium between the ions and the two parent compounds: the reduced and oxidized form. Let the concentrations of these two forms be c_r and c_o, that of the ions of either sign c_i, then in equilibrium

$$c_i^2 = K c_r c_o \qquad (I)$$

with K = equilibrium constant. If the solution is diluted with the pure solvent in a ratio r:1, both c_r and c_o are reduced by the same factor; hence the new ion concentration c_i' is given by

$$c_i'^2 = \frac{K}{r^2} c_r c_o$$

or

$$c_i'/c_i = 1/r. \qquad (II)$$

A thermodynamic equilibrium thus leads to a conductivity proportional to the dilution ratio $1/r$.

Second, it is possible that the above equilibrium constant K is so small that practically no ions are produced thermodynamically. This is another way of saying that the basic strength (ability of accepting a proton) of the oxidation product of catechol is too small. Practically nothing is known of the basic strength of *o*-quinones; Egerton and McLean (4), in agreement with others, found that *p*-quinones are very weak bases. Even in this case, ions may be generated kinetically in the process of oxidation. These ions are then not absolutely stable, but may be so relatively. This is possible if the path in reverting from the ion to the stable form leads through a potential hump that slows down the conversion rate to an appreciable degree. Ions of this type, clearly different from those resulting from an electrolytic dissociation, will be called oxidative ions in the present connection. Ions present in the solution by this mechanism are reduced proportionally to the factor $1:r$, if the solution is diluted in a ratio r:1. Hence the same conductivity-dilution relation must prevail as in the previous case. Discrimination between the two possibilities by means of dilution tests is not possible.

It can be shown that equation (II) holds in a first approximation for oxidized catechol solutions. Fig. 6 presents on a bilogarithmic scale conductivity σ as a function of dilution ratio r. A dotted line, curve 3, indicates the slope for $\sigma \sim 1/r$. The two experimental curves, for benzene and oil, are, with regard to their slope, close to the dotted line. Acid-amine-phenol

solutions show quite differently shaped, downward convex dilution curves (1). Curves from strong acids in dielectric solvents (3) are also convex toward the abscissa, σ at low concentrations varying with the square root of the acid concentration.

While it is not possible on the above basis to differentiate between the two possible mechanisms of ion generation, there are a number of other observations which are in favor of the second mechanism producing oxidative type ions. These observations will be discussed later. It is understood, however, that a definite conclusion in this regard will need further experimental work.

Instability of Oxidative Ions

It was observed that in several combinations, although not in all, the solution decanted from the solid oxidant showed a conductivity decreasing with time. Fig. 7 presents two examples of this behavior. On several samples, tested after standing a number of days, the conductivity still showed a high level. Although such behavior is observed in other dielectric liquids also, it may be interpreted as indicating the presence of oxidative ions which, as explained, are not absolutely stable.

The instability is more striking if iodine is used as an oxidant, the iodine being, of course, in solution. As a result of oxidation, the iodine is reduced to hydriodic acid which is a strong acid and soluble in xylene in small concentrations; its effect on the conductivity must be taken into consideration.

From acid number measurements, the percentage of I_2 undergoing reduction was estimated. A 0.2 millimole per liter I_2 solution in xylene had an acidity of $0.06 \times 10^{-3}N$; a 3 millimole per liter butylcatechol solution, $0.23 \times 10^{-3}N$. A solution containing both had an acidity of $0.38 \times 10^{-3}N$, a net increase of $0.09 \times 10^{-3}N$, which corresponds to about 25 per cent of the iodine added.

Next, the conductivity due to HI in xylene was determined (Fig. 8). Although this is a flat S-shaped curve, the average slope corresponds closely to $\sigma \sim \sqrt{c_{HI}}$, as mentioned before; strong acids behave as typical weak acids in hydrocarbons.

Fig. 9, curve 1, shows the time dependence of σ for a xylene solution of 0.16 millimole per liter I_2 and 3.2 millimole per liter butylcatechol. The amount of HI present is about $0.08 \times 10^{-3}N$, corresponding (Fig. 8) to $\sigma = 0.5 \times 10^{-12}$ mho/cm. The excess of σ for curve 1 above that level is then due to oxidative ions of the catechol. They can be seen to be relatively unstable, in contrast to the ions from HI, shown by curve 2, the concentration of which for the same time of 30 minutes decreases to a much lesser degree.

In this connection another observation may be quoted, namely the increase in conductivity upon addition of picric acid to a catechol solution (Fig. 10). The two are known to form an addition compound,

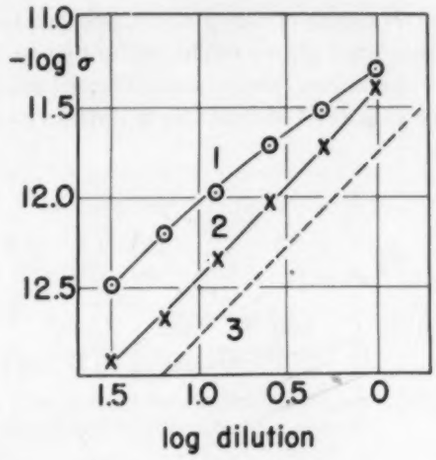

Fig. 6. Conductivity vs. dilution ratio. Curve 1—butylcatechol 3.5 millimole/liter, benzene; curve 2—butylcatechol 4.5 millimole/liter, hydrocarbon oil; curve 3—45-degree line.

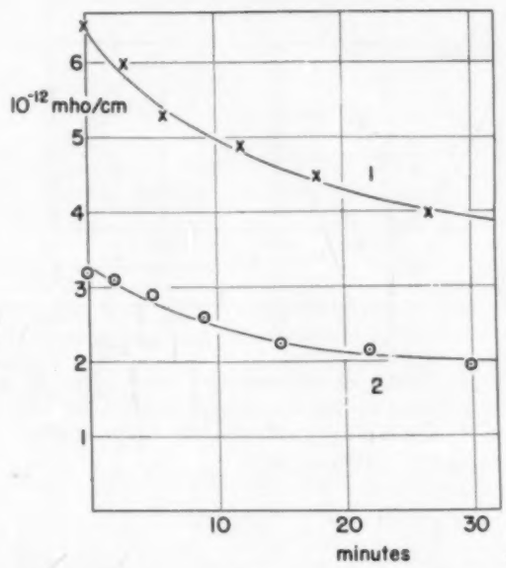

Fig. 7. Decay of conductivity with time for 3 millimole/liter butylcatechol, oxidized with permanganate. Curve 1—*n*-heptane; curve 2—benzene.

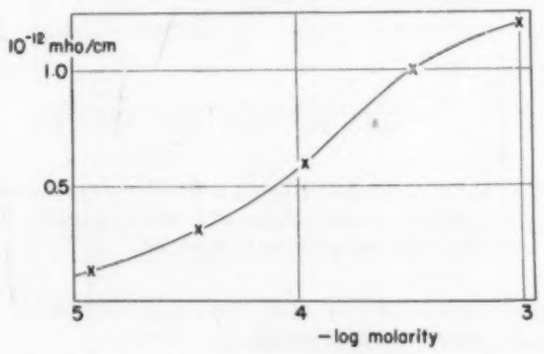

Fig. 8. Conductivity vs. concentration of HI in xylene

and, in the course of this process, positive ions of the type postulated above might be formed in the presence of the strong picric acid. These ions are very unstable as curve 1 shows. Curve 2 refers to a control

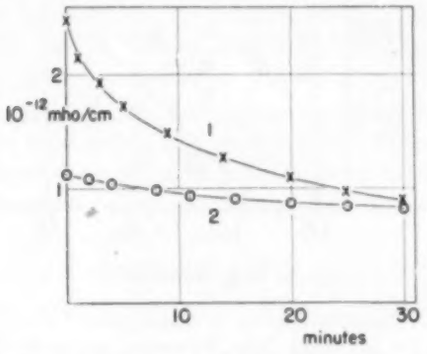

FIG. 9. Decay of conductivity with time in xylene solutions. Curve 1—iodine 0.16 millimole/liter, butylcatechol 3.2 millimole/liter; curve 2—HI 1.3 millimole/liter.

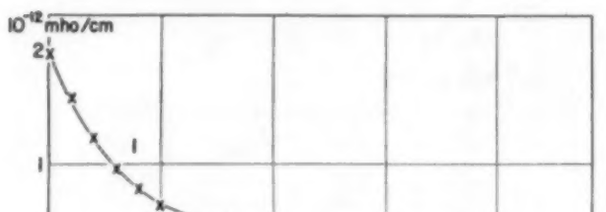

FIG. 10. Decay of conductivity with time in xylene solutions. Curve 1—butylcatechol 2.6 millimole/liter, picric acid 0.17 millimole/liter; curve 2—butylcatechol none, picric acid 0.17 millimole/liter.

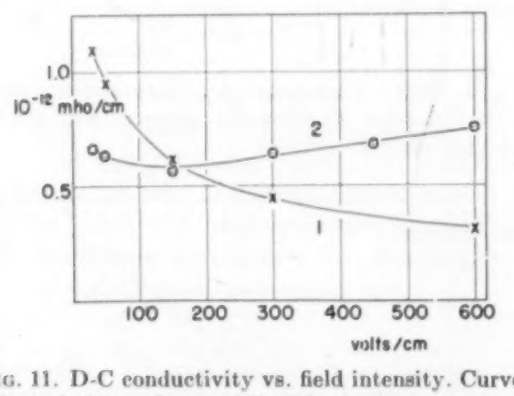

FIG. 11. D-C conductivity vs. field intensity. Curve 1—butylcatechol in xylene, oxidized by permanganate; curve 2—acid-amine-phenol solution in benzene.

test containing picric acid only; σ is seen to be of a much lower level and stable.

D-C Polarization

In measuring the conductivity with direct current instead of alternating current, as in all previous measurements, decreasing conductivity with increasing field intensity is observed, if the original level of conductivity is 10^{-12} or less (see curve 1 of Fig. 11). The initial value, corresponding to the lowest field of 30 volts/cm is some 20 per cent lower than the a-c value. From then on, σ decreases markedly in a range of moderate field intensities. Each value is fairly constant with regard to time. Such a decrease is due to polarization because of the limited number of ion pairs between the electrodes. Ions accumulate near the electrodes of opposite sign; an equilibrium is reached between ion migration in the electric field and diffusion in the opposite direction. Because of the resulting nonlinear potential drop there is an apparent increase of total resistance, more so the higher the current density. For conductivities of around 10^{-11} this polarization was not observed.

In case the ion concentration is immediately restored by electrolytic dissociation, such an effect does not take place. This is shown by curve 2 of Fig. 11, referring to an acid-amine solution. After a flat minimum there is a gradual increase of σ with increasing field, a behavior usually encountered in dielectrics (increase of ionic mobility).

TABLE II. *Effect of further addition of catechol on conductivity*

Concentration of butylcatechol in benzene, millimole/liter	Conductivity, 10^{-12} mho/cm
1.2	6.0
1.9	5.2
2.6	4.9
4.0	4.9
6.1	5.2
9.6	5.7

The d-c polarization as observed can be construed as due to a limited number of ion pairs, consistent with oxidative ion generation.

Role of Catechol and o-Quinone Concentration

If all ions were in thermodynamic equilibrium with catechol and its chief oxidation product, *o*-quinone, the concentration of these two should determine the conductivity. Certain experiments were carried out in this respect, and they seem to indicate that this is either not the case or is to only a limited extent.

Table II shows results from a continued addition of butylcatechol to a permanganate-oxidized benzene solution. There is no significant change in σ, indicating that the ion concentration is determined rather by the previous oxidation process.

In another experiment the effect of *o*-quinone was checked. The latter was prepared from catechol according to Willstätter and Pfannenstiel (5), and its

conductivity-concentration diagram in dioxane containing 3.6 millimole per liter catechol was established (Fig. 12). There is a pronounced increase of σ, indicating that there is a certain ion concentration determined by equilibrium. The next question was what part this effect played in the oxidation tests.

Fig. 13, curve 1, shows a σ vs. time relation for catechol in dioxane. Next, it was necessary to establish the quinone concentration for each point. This was done by means of a Klett photoelectric colorimeter, using a blue filter. In a separate test, a calibration curve (not shown) between quinone concentration and optical density was established. From the optical density of the solution (curve 1, Fig. 13) at the times shown, the quinone concentration was determined. Fig. 12 now was used; from that curve the conductivity at each quinone concentration was read. These conductivity data were plotted in curve 2, Fig. 13. This shows that the total change in σ due to *o*-quinone present is only about 12 per cent; the major part of the effect must be due to oxidative ions.

In certain combinations, for instance catechol in benzene, very pronounced oxidation takes place by silver oxide (2) so that the quinone concentration is high; yet the increase in conductivity is small. All these results show that the ion concentration is determined rather by the path that the oxidation process takes, depending on whether it leads through ionic stages that persist to a certain extent.

Temperature of Oxidation

It appeared to be of interest to conduct oxidation tests at different temperatures. Results of such a series are shown in Fig. 14 for butylcatechol in xylene. All conductivities were measured at 25°C, the oxidation being carried out at temperatures ranging from zero C to 75°C. The result seems to show that at zero C, as well as at 50° and 75°C, the conductivity levels reached are lower than at 25°C. This observation needs further experimental verification, but a tentative explanation may be given as follows. Oxidation rate increases with increasing temperature, hence the σ-levels should also increase with rising oxidation temperatures. It is possible, on the other hand, that the higher the temperature, the more direct the oxidation, without going through intermediate ionic stages. In this manner an optimum temperature for the σ-level might result, which may well be in the neighborhood of room temperature. This observation is, therefore, also in keeping with the concept of oxidative ions.

Chemical Structure of Oxidative Ions

Up to this point nothing was said about the possible chemical structure of the cation, except that it

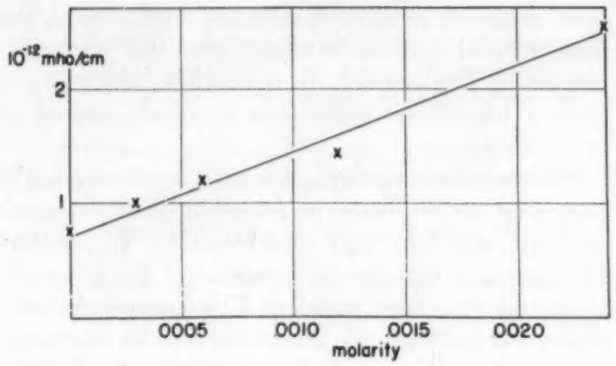

Fig. 12. Conductivity vs. concentration for *o*-quinone in dioxane, containing 3.6 millimole/liter catechol.

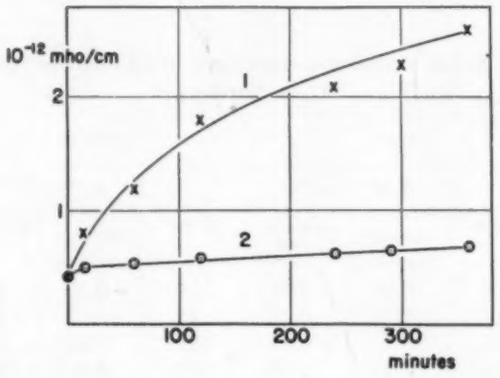

Fig. 13. Conductivity vs. oxidation time for 4.5 millimole/liter catechol in dioxane, oxidized by $KMnO_4$. Curve 1—observed data; curve 2—plotted after Fig. 12, from *o*-quinone produced.

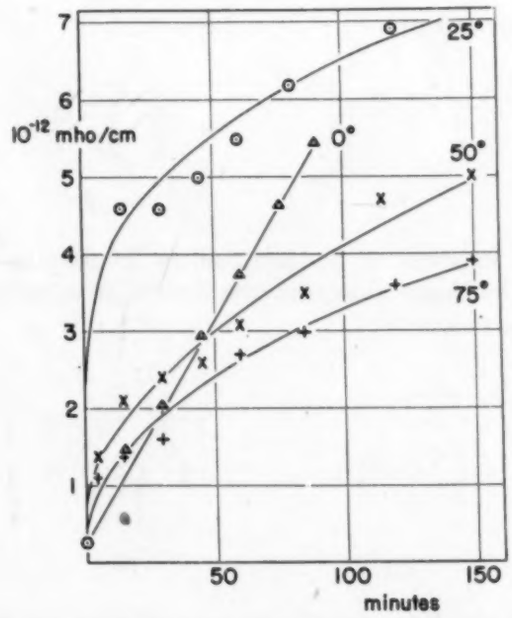

Fig. 14. Conductivity vs. oxidation time at different oxidation temperatures as shown. 3.5 millimole/liter butylcatechol in xylene, oxidized by $KMnO_4$. All conductivities measured at 25° C.

is an oxidation product of catechol. And, indeed, the experimental material does not permit a final conclusion in this respect. It is possible, however, to form a hypothesis which has a certain degree of probability.

Whereas the main oxidation product of catechol is *o*-quinone, an intermediate oxidation product, quinhydrone, was long ago established by Willstätter. The generally bimolecular structure of the latter for all quinones has been questioned by various authors, Weitz, for instance (6). Elema as well as Michaelis (7) proved experimentally for some quinones that the intermediate form, called semiquinone, is monomolecular. The existence of monomolecular intermediate forms can be considered as definitely established.

TABLE III. *Comparison between catechol and hydroquinone in diozane*

Ag_2O			$KMnO_4$		
Time in min	σ, 10^{-12} mho/cm		Time in min	σ, 10^{-12} mho/cm	
	Catechol	Hydroquinone		Catechol	Hydroquinone
0	0.40	0.31	0	0.30	0.31
30	1.5	0.15	45	0.75	0.18
60	5.1	0.15	105	0.83	0.20
120	9.2	0.18	270	1.4	0.28

If one tries to use this concept for catechol, a difficulty arises. The pertinent electronic structure of catechol (I) and *o*-quinone (II) is shown below.

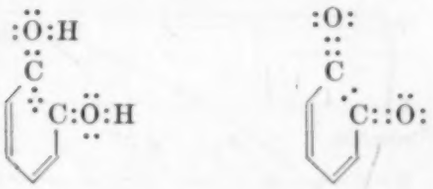

I II

The structure of the semiquinone, containing only one hydrogen atom, may be derived from either of these two, thus:

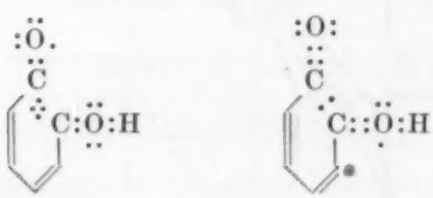

III IV

Both structures contain an unpaired electron; hence both are free radicals and must be rather unstable. Both, however, must considerably increase in stability, if to III an electron is added and from IV an electron is removed, thus:

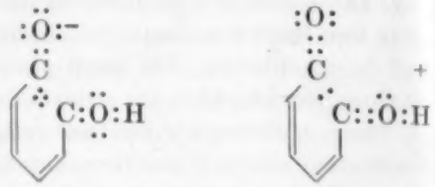

V VI

In these two saturated structures possessing completed octet shells throughout, V is a negative, and VI a positive ion, the first having benzenoid, the second quinonoid structure; both are electrically charged semiquinones of appreciable stability. The first is the monovalent anion of catechol, which is a weak acid, while the second is the cation of an *o*-quinone, which has accepted a proton. One might picture also bivalent ions of this kind. These structures fit as a special case into the general mechanism of ion generation described previously.

As mentioned before, no noticeable ion formation can be expected from mixing the two compounds. They might form, however, as intermediate oxidation stages. The oxidation of catechol, which may be described by a reaction such as:

$$C_6H_4(OH)_2 + O = C_6H_4O_2 + H_2O,$$

then takes place to a certain fraction in two ionic stages, thus:

$$C_6H_4(OH)_2 + O = C_6H_4O(OH)^+ + (OH)^-$$

$$C_6H_4(OH)_2 + (OH)^- = C_6H_4(O\bar{H})O^- + H_2O,$$

resulting in a quinonoid cation and a benzenoid anion. The two ions may partly recombine, forming one molecule of quinone and one of catechol, but may partly persist for a long time as relatively stable oxidative ions.

These ionic formulas were derived from monomer molecules, but similar considerations would hold if the molecules were dimers, tetramers, or the like.

Comparison of Ortho- and Para-Compounds

One might ask whether the described conductivities are observable with para-compounds as well. Some experimentation along this line gave a negative answer to the above question, as Table III shows, referring to a comparison between catechol and hydroquinone, 4.5 millimole per liter in dioxane, using Ag_2O and $KMnO_4$ as oxidants.

The reason for this difference is probably the same that causes the oxidation rate of catechol to be altogether higher than that of hydroquinone. As may

be seen from the structural formulas, a change from I to II involves only two carbon atoms, whereas a corresponding change in para-compounds involves the entire ring. It appears that not only the oxidation rates differ, but also the fraction that follows an oxidation path along ionic stages is larger for ortho- than para-compounds.

Any discussion of this paper will appear in a Discussion Section, to be published in the June 1954 issue of the JOURNAL.

REFERENCES

1. A. GEMANT, Conference on Electrical Insulation, National Research Council, Lenox, October 1952.
2. E. DYER AND O. BAUDISCH, *J. Biol. Chem.*, **95**, 483 (1932).
3. A. GEMANT, *J. Chem. Phys.*, **12**, 79 (1944).
4. L. EGERTON AND D. A. MCLEAN, *Ind. Eng. Chem.*, **38**, 512 (1946).
5. R. WILLSTÄTTER AND A. PFANNENSTIEL, *Ber.*, **37**, 4744 (1904).
6. E. WEITZ AND E. MEITZNER, *Ber.*, **64**, 2909 (1931).
7. L. MICHAELIS AND M. P. SCHUBERT, *Chem. Revs.*, **22**, 437 (1938).

Formation of Immersion Zinc Coatings on Aluminum[1]

W. G. Zelley

Aluminum Research Laboratories, Aluminum Company of America, New Kensington, Pennsylvania

ABSTRACT

It has been recognized for many years that aluminum and its alloys require specific surface preparation for successful electrodeposition of the various metals. Such special treatment is necessary because of the high position of aluminum in the electromotive force series and because of the relatively impervious and rapidly formed oxide film. Many procedures for plating on aluminum have been presented in the literature, most of them falling into one of the following categories: (*a*) surface roughening or roughening plus heavy metal deposition by immersion prior to electroplating; (*b*) anodic oxidation followed by electrodeposition in the pores of the coating; (*c*) direct zinc plating prior to plating with other metals; (*d*) immersion deposition of zinc prior to plating with other metals. The zinc immersion procedure is now considered the most practical and economical of the various processes and, accordingly, has the greatest commercial application. In general, this procedure requires less time and equipment, is less critical to control, and has wider applicability than other known methods.

Growth of Zinc Immersion Process

An alkaline zinc immersion bath was patented by Hewitson (1) in 1927, and zinc immersion procedures were employed by Altmannsberger (2) in 1931 and 1932, by Braund and Sutton (3) in 1935, by Elssner (4) also in 1935, and by Layner and Orlova (5) in 1936. Later patents were issued to Korpiun (6) in 1939 and Perner (7) in 1942. The zinc immersion process, however, was not widely applied until relatively recent years, during which significant work has been reported by Bengston (8), Meyer (9, 14), Ehrhardt and Guthrie (10), Bullough and Gardam (11), Heiman (12), Keller and Zelley (13, 15), and Bailey (16). While good commercial plating on aluminum is now entirely feasible, further study into the mechanism of the process may result in a still more improved plated surface, especially with regard to resistance to corrosion.

Corrosion of Plated Aluminum

The zinc immersion process, or any process involving a layer of zinc between the aluminum and the electrodeposit, introduces a specific corrosion problem. In many environments zinc is anodic to aluminum; consequently, it tends to protect both the aluminum and the electrodeposit. This results in undercutting at the interface, and subsequent blistering and flaking of the deposit. Thus, while plated steel, for example, may fail by rusting, the rust spots usually can be removed by polishing and the original appearance restored. However, a plated aluminum surface that has blistered is permanently defaced.

A suggested mechanism for this type of corrosion is diagramatically illustrated in Fig. 1. Item (a) shows the cross section of a plated aluminum surface that has been grooved to the base metal, thus exposing aluminum, zinc, and electrodeposit to the corrosive environment. In item (b) the zinc has protected the electrodeposit and the aluminum by self-sacrifice until the throwing power of the reaction has been exceeded. At this point, item (c), aluminum protects the electrodeposit by self-sacrifice until zinc is again exposed. Starting with item (d), the cycle repeats itself. Undercutting of the deposit in this manner becomes evident by the appearance of blistering and lifting. Fig. 2 is a photograph of the cross section of a corroded, grooved sample demonstrating this type of lifting.

Consideration of such mechanism results in the following conclusions on the performance of plated aluminum:

1. The thinnest practicable zinc film produces the best corrosion results, for it permits the least lateral penetration before the throwing power is exceeded.
2. Those aluminum alloys with the lowest solution potentials provide the most resistant plated products. Thus, 24S alloy should be better than 2S alloy because of a lower potential difference between base metal and electrodeposit.
3. Large breaks in the deposit are less harmful than small, because small breaks furnish a correspondingly small anode area to protect the electrodeposit. Therefore, attack is more rapid, and blistering and lifting occur earlier. For this reason stress cracks, such as might appear on bright nickel plate, are very harmful, and bright plating baths must be operated with caution.

[1] Manuscript received November 10, 1952. This paper was prepared for delivery before the Montreal Meeting, October 26 to 30, 1952.

4. Finally, any modification of the immersion deposit that decreases the rate of solution of zinc by the anodic reaction would be beneficial.

As early as 1927, Work (17) plated on a smooth aluminum surface by applying a thin electrodeposit of zinc prior to plating with other metals. Such plated aluminum had excellent appearance and good adhesion but failed rapidly in corrosion tests. Work could overcome this rapid corrosion only by employing a heat treatment, a step which is objectionable commercially. The zinc film was apparently the source of the difficulty, and although Work specified the thinnest zinc layer which he believed practicable, it still was considerably thicker than present immersion deposits. In like manner, poor results attributed to the zinc immersion process may often be traced to the properties of the immersion film.

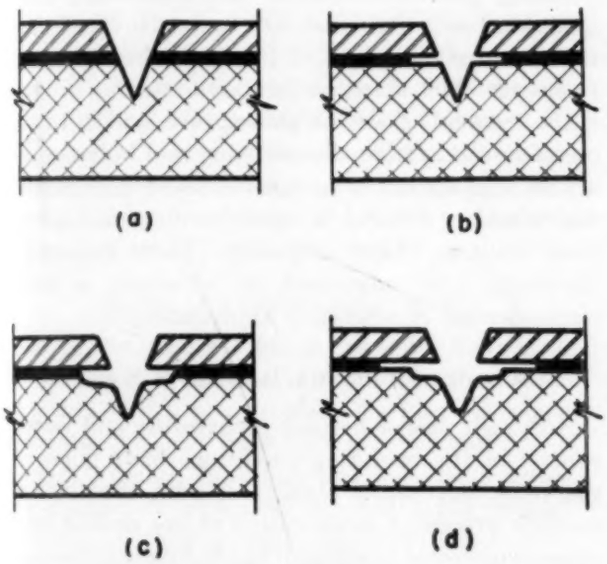

FIG. 1. Corrosion mechanism of aluminum plated by the zinc immersion process.

DEPOSITION OF THE ZINC FILM

One of the reasons that zinc has been so successful for immersion deposits on aluminum is its relative proximity to aluminum in the electromotive force series of metals. Indeed, the relative order of the two metals is interchangeable, depending on the environment. Metals further removed from aluminum in this series are more difficult to deposit by immersion, such deposits usually tending to be granular and nonadherent.

It is understandable then that the potential difference between zinc and aluminum, in a given immersion bath, would determine to a large extent the weight and character of the zinc deposited. Since the zinc film is so important in the resistance to corrosion of electroplated aluminum, this potential difference becomes a very significant property. In general, the zinc-aluminum potential difference, in a given immersion bath, depends on two factors: (*a*) the particular aluminum alloy in question; and (*b*) the surface conditioning treatment employed on that alloy.

Choice of alloy is important because of the inherent differences in solution potential among the various aluminum alloys. Thus, in alkaline immersion baths, 2S has a greater potential difference with respect to zinc than does 24S-T3. Consequently, the increased

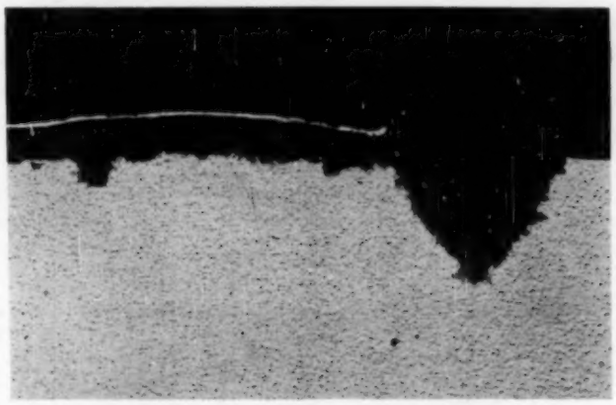

FIG. 2. Cross section through grooved plated panel after salt spray exposure. Shows undercutting and lifting of the deposit. 20×.

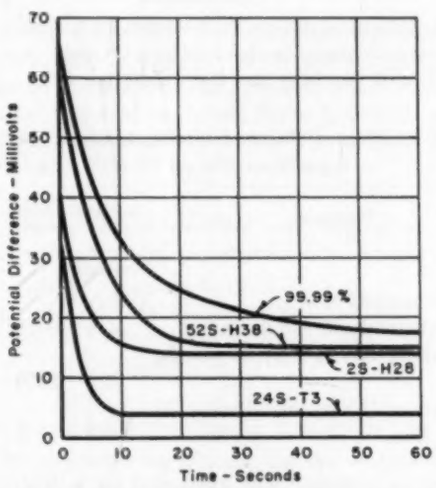

FIG. 3. Potential difference between various aluminum alloys and high purity zinc in a solution of 500 g NaOH per liter and 100 g ZnO per liter.

driving force of the immersion reaction results in a heavier film of zinc on the 2S. Fig. 3 is a graph of zinc-aluminum potential difference for various aluminum alloys. This graph does not purport to show absolute potential differences, but rather it indicates relative initial values and the intervals of time to reach a steady value, as determined with a recording potentiometer.

Usually, however, the alloy is specified according to other requirements, and it may be necessary to

plate on one with adverse potential properties. It is then that surface conditioning becomes particularly important. By selecting the proper pretreatment it is frequently possible to decrease markedly the potential difference between zinc and the aluminum alloy. For example, a double immersion treatment on 2S provides a lower zinc-aluminum potential difference and a lower weight of zinc than does mild alkaline cleaning. In turn, mild alkaline cleaning results in a lower zinc-aluminum potential difference than does

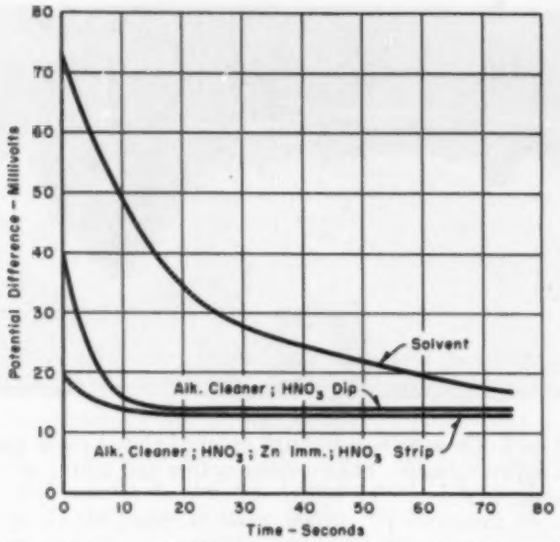

FIG. 4. Potential difference between 2S-H28 with various conditioning treatments and high purity zinc in a solution of 500 g NaOH per liter and 100 g ZnO per liter.

TABLE I. *Effect of the conditioning treatment on the zinc immersion film on 2S-H28*

Treatment	Coating wt.	Zinc content	Resistance*
	mg/dm²	%	*microhms*
Electrodeposited zinc			5
Solvent cleaned; 30 sec Zn imm.†	15.8	93.8	10
Alk. cleaner; HNO_3 dip; 30 sec Zn imm.	5.3	83.0	15
Alk. cleaner; HNO_3 dip; double 30 sec Zn imm.	2.5	72.5	70

* Surface resistance was measured by a Kelvin Bridge using 0.25 in.² contacts and 500 lb pressure.

† The zinc immersion solution had a composition of 500 g of NaOH per liter and 100 g of ZnO per liter.

solvent degreasing. Fig. 4 shows qualitatively the zinc-2S aluminum potential difference for various conditioning treatments. The zinc-aluminum potential difference varies with the conditioning treatment apparently because of the nature of the film formed by the treatment, the effect of the treatment on constituents and surface irregularities, or a combination of these factors.

Extremely thin zinc deposits, such as produced by a double immersion treatment, are not continuous films of pure zinc. This condition is not detrimental as long as there is sufficient zinc to provide satisfactory electrodeposition and is definitely beneficial from a corrosion point of view. Both chemical analysis and contact resistance measurements have been employed to indicate the nature of the zinc film. For an electroplated or heavy immersion zinc coating the resistance is low and the percentage of metallic zinc is high. As the film becomes thinner, however, the resistance increases and the percentage of zinc decreases. Table I summarizes contact resistance and zinc analysis data for various weights of coating.

Of course, time and temperature of immersion also affect the weight of zinc deposited, although their relative importance frequently depends on the conditioning treatment selected. It is a good policy, however, to maintain these variables as low as conveniently practicable. While the conditioning treatment has been considered with respect to its effect on the zinc coating weight, it has two other important functions which must be fulfilled first. One of these is the removal of all the grease, dirt, and disturbed metal resulting from the polishing and buffing operations. The second is to remove those constituents which are not covered in subsequent operations and thus result in blister formation. These factors are obviously very important for obtaining a sound electrodeposit of attractive appearance.

Modification of the Immersion Solution

Although proper surface preparation and careful control of the operating conditions have improved markedly the results obtainable with the zinc immersion process, a modification of the zincate bath[2] appears desirable to utilize it to the fullest advantage.

For example, while the "double immersion" technique has been shown to produce a low weight of zinc, it does not always completely overcome the effect of constituents on magnesium and magnesium silicide type of alloys. Also, on 2S alloy it is sometimes possible to so reduce the weight of zinc by means of the double immersion that the surface resistance is too high for satisfactory coverage by the plating bath.

The addition of a small amount of ferric chloride, maintained in solution by the tartrate ion, has proved to be very beneficial to the zincate bath. Not only does it increase the effectiveness of the double immersion treatment on magnesium-containing alloys, but it also provides for more consistent electroplating coverage on all other alloys. Furthermore, double immersion from this modified solution has improved the plating of die castings to the extent that

[2] The modified zinc immersion procedures are the subjects of pending patent applications.

items on which the standard techniques have failed are often successfully finished.

A small amount of iron can be detected in the immersion film deposited by the modified zincate bath. The resistance to corrosion of aluminum plated with this type of film is improved for most of the alloys, notable exceptions being 24S and 75S. Improvement in corrosion properties is possibly a function of the percentage of metallic zinc in the modified film and its consequent effect on the anodic solution of that film. Fig. 5 demonstrates the increased resistance to corrosion that can be obtained with a modified zinc immersion.

Usually, 1 to 2 g of ferric chloride crystals are employed per liter of immersion bath, and approximately 10 g of Rochelle salt per gram of ferric chloride crystals will maintain the iron in the highly alkaline solution. A large excess of ferric chloride is to be avoided, for it results in blistering of the electrodeposit. With alloys of high magnesium content it may also be of value to increase the Rochelle salt content to 100 g/l. The modified solution is prepared by dissolving the zinc oxide in concentrated sodium hydroxide in the usual manner, then adding the iron as a water solution of ferric chloride and Rochelle salt. Composition of the solution is shown in Table II.

Dilute Immersion Solutions

Most of the zincate baths in use today have basic compositions of 400–500 g of sodium hydroxide per liter and 80–100 g of zinc oxide per liter. Excellent results are obtained from this type of bath. It is extremely viscous, however, and has the inherent disadvantages of high drag-out and being difficult to remove by rinsing. Such characteristics become especially critical when it is desired to use automatic equipment. Various immersion solutions, less concentrated than the above described bath, have been reported in the literature, but, in general, the concentrated baths have been considered more reliable.

In any sodium zincate solution there is a minimum amount of sodium hydroxide necessary for the given quantity of zinc oxide. This sodium hydroxide content, which is in excess of the amount theoretically required to react with the zinc oxide, is necessary to prevent precipitation of zinc hydroxide. The more dilute the solution, the greater must be the ratio of sodium hydroxide to zinc oxide. For example, in a one liter solution the following ratios are commercially practical: 400 g NaOH for 100 g ZnO; 120 g NaOH for 20 g ZnO; 50 g NaOH for 5 g ZnO. The last two are possible dilute solutions.

Experimental work on the weight of the zinc film indicates that this value may be fundamental in the less satisfactory performance frequently encountered with dilute baths, for the weight of the zinc film tends to increase appreciably upon dilution of the immersion solution. The weight of zinc deposited from a dilute immersion would be expected to be a function of the potential difference between zinc and the aluminum surface in like manner to that previously described for concentrated immersions. Consequently, to decrease the coating weight it is necessary to adjust the solution or vary the conditioning treatment, thereby decreasing that potential difference.

Sodium nitrate and Rochelle salt are two important additions to dilute immersion solutions. Suitable sodium nitrate additions are on the order of 0.5 to 1.0 g/l, and in many cases reduce the coating weight by 30–50 per cent. An excess must be avoided, however, for as much as 2 g/l may result in a zinc

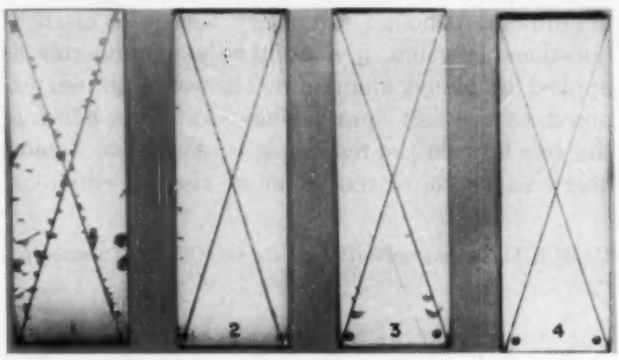

Fig. 5. Panels prepared with regular and modified zinc immersions after 300-hr exposure to the salt spray. Panel 1, 3S-H16 regular immersion bright nickel; panel 2, 3S-H16 modified immersion bright nickel; panel 3, 61S-T6 regular immersion Watts nickel; panel 4, 61S-T6 modified immersion Watts nickel.

TABLE II. *Composition of modified zinc immersion solution*

g/l	
500	Sodium hydroxide
100	Zinc oxide
1	Ferric chloride crystals
10	Rochelle salt

film with a contact resistance too high for good coverage by subsequent plating baths. Rochelle salt aids in conditioning magnesium and magnesium silicide type alloys as well as in providing low coating weights. Likewise, dilute baths can be modified with the iron addition in the same manner as a concentrated solution. This markedly improves the resistance to corrosion of the electroplated aluminum and, except on 24S and 75S alloys, is undoubtedly the most important single additive.

Surface preparation should be especially thorough when employing dilute immersion solutions. Most of the more effective conditioning treatments are applicable and the double immersion technique is of particular value. Also, time and temperature of immersion are more critical with dilute zincate

solutions, and it is desirable to limit the immersion to a maximum of 30 seconds at a temperature of not over 75°F.

Probably the most practical dilute immersion bath for commercial operation would have a basic composition of 120 g/l NaOH and 20 g/l ZnO. This solution results in a relatively small increase in rinsing and drag-out properties over more dilute baths, yet at the same time it provides a greater reserve of zinc. Table III gives the complete composition of such a bath.

Performance of Plated Aluminum

The two most widely used corrosion tests, namely salt spray and atmospheric exposures, have been employed in the evaluation of electrodeposits on aluminum. Although salt spray testing is often of questionable value, it does have a definite role as applied to plated aluminum. Grooved samples exposed to the salt spray demonstrate the effect of the zinc film on the resistance to corrosion. Atmospheric exposure, of course, must also be employed to obtain complete data on the outdoor life expectancy of plated parts.

TABLE III. *Composition of dilute modified zinc immersion solution*

g/l	
120	Sodium hydroxide
20	Zinc oxide
50	Rochelle salt
2	Ferric chloride crystals
1	Sodium nitrate

Interest in the performance of plated high strength aluminum alloy articles has resulted in the accumulation of considerable information on decorative chrome plated 24S-T4. Since 24S-T4 is a very favorable alloy on which to plate by the zinc immersion process, excellent resistance to corrosion can be obtained. Ordinarily, with 0.0015 in. nickel under the chromium, plated 24S-T4 would be expected to satisfactorily withstand at least three years' exposure in an industrial atmosphere.

The inherent properties of 24S-T4 alloy make it possible to obtain good results on this alloy without any special precautions in the zinc immersion bath. Other alloys are not so readily treated, but the application of the principles discussed above will produce good results on them as well. For example, 2S was included in another plating exposure program together with 24S-T4, brass, steel, and zinc. The 2S was plated using a double immersion from a modified solution, while the other metals were prepared according to best standard practices. It is significant that, after three years in the New Kensington, Pennsylvania, atmosphere, plated 2S is as good as the plated 24S-T4, and the plated aluminum compares favorably with the plated brass, steel, and zinc samples.

Recently there has been increased interest in plated aluminum die castings. As yet there is less background information on die castings, and unquestionably they are more difficult to plate satisfactorily than wrought alloys. One of the difficulties in the plating of die castings results from the greater percentages of copper, silicon, and magnesium usually found in casting alloys. However, the factors affecting the zinc immersion film appear to be more critical for castings than for wrought material. Use of the modified immersion solution seems to offer some advantage for castings. Casting alloys currently under consideration for plated finishes are No. 360, 380, and 218 alloys. While procedures have been developed for all three alloys, alloy 380 is probably the most suitable for electrodeposition. The plated finish on die castings of this alloy, when applied according to the best known methods, should withstand an industrial atmosphere for at least one year.

Summary

To obtain corrosion resistant electrodeposits on aluminum, it is necessary to obtain good coverage on the thinnest possible zinc film. The surface conditioning treatment is important in this objective by removing dirt and grease, dissolving interfering constituents, and providing a surface with favorable potential properties. An addition of iron to the immersion bath itself aids materially in improving coverage and in decreasing the corrosion reaction in the zinc film. Dilution of the immersion bath introduces additional problems and, in general, necessitates closer control over surface preparation and operating conditions. Sodium nitrate and Rochelle salt, as well as the iron, have been employed as additions to dilute baths. By exercising a few precautions it is possible to obtain good service performance of plated finishes on wrought aluminum alloys. Casting alloys present a somewhat more difficult problem, but careful treatment should provide relatively good results in this field as well.

Any discussion of this paper will appear in a Discussion Section, to be published in the June 1954 issue of the Journal.

REFERENCES

1. E. H. Hewitson, U. S. Pat. 1,627,900, May 10, 1927.
2. K. Altmannsberger, *Chem. Ztg.*, **55**, 709 (1931); **56**, 247 (1932).

3. B. K. Braund and H. Sutton, *Trans. Faraday Soc.*, **31**, 1595 (1935).
4. G. Elssner, *Aluminium*, **17**, 376 (1935).
5. V. I. Lainer and S. I. Orlova, *Legkie Metall.*, **5**, No.2, 22 (1936).
6. J. Korpiun, U. S. Pat. 2,142,564, January 3, 1939.
7. L. Perner, U. S. Pat. 2,297,241, September 29, 1942.
8. H. Bengston, *Trans. Electrochem. Soc.*, **88**, 307 (1945).
9. W. R. Meyer, *Monthly Rev. Am. Electroplaters' Soc.*, **33**, 269 (1946).
10. R. A. Ehrhardt and J. M. Guthrie, *Monthly Rev. Am. Electroplaters' Soc.*, **34**, 421 (1947).
11. W. Bullough and G. E. Gardam, *J. Electrodepositors' Tech. Soc.*, **22**, 169 (1947).
12. S. Heiman, *J. Electrochem. Soc.*, **95**, 205 (1949).
13. F. Keller and W. G. Zelley, *Ann. Proc. Tech. Sessions Am. Electroplaters' Soc.* (1949).
14. W. R. Meyer and S. H. Brown, *Ann. Proc. Tech. Sessions Am. Electroplaters' Soc.* (1949).
15. F. Keller and W. G. Zelley, *J. Electrochem. Soc.*, **96**, 143 (1950).
16. G. L. J. Bailey, *J. Electrodepositors' Tech. Soc.*, **27**, 233 (1951).
17. H. K. Work, *Trans. Electrochem. Soc.*, **53**, 361 (1928).

Polarography of Thioglycolic Acid[1]

D. L. Leussing and I. M. Kolthoff

School of Chemistry, University of Minnesota, Minneapolis, Minnesota

ABSTRACT

Thioglycolic acid exhibits polarographic behavior at the dropping mercury electrode similar to cysteine and glutathione. A reversible anodic wave is found, the characteristics of which correspond to the formation of a mercurous thioglycolate complex. This wave is suitable for the analysis of thioglycolic acid in solutions. A second irreversible anodic wave probably is due to the formation of an insoluble mercuric monothioglycolate. The standard potential of the electrode reaction has been calculated from the experimental results. Dithiodiglycolic acid is irreversibly reduced to thioglycolic acid at the dropping mercury electrode. Calculated diffusion coefficients of various species from polarographic data are given.

Introduction

Following a report from this laboratory[2] on the polarographic properties and determination of thioglycolic acid, a paper was published on the same subject by Liberti and Cervone (1). The results in the two papers differ in various minor respects and in a major respect regarding the interpretation of the reaction mechanism. The interpretation in the report is in agreement with that of Kolthoff and Barnum (2) for cysteine and with Stricks and Kolthoff (3) for reduced glutathione.

Larsson (4) reports values for the acid dissociation constants of thioglycolic acid to be 2.1×10^{-4} for K_1 and 2.1×10^{-11} for K_2 at 25°C. In this laboratory, Bush (5) titrated thioglycolic acid with sodium hydroxide using a glass electrode. From his data and using approximate ion activity coefficients as tabulated by Kielland (6), the values for the activity constants were calculated to be 2.5×10^{-4} and 2.8×10^{-11} at 25°C. These values are used in the calculations in this paper.

The polarography of dithiodiglycolic acid was briefly investigated.

Experimental

Purification of thioglycolic acid.—Thioglycolic acid of 99.8 per cent purity by an analysis to be described below was prepared by twice vacuum distilling Eimer and Amend "pure" thioglycolic acid. The fraction collected boiled at 95°–96°C at 8 mm pressure. A purity of about 99 per cent was obtained after one vacuum distillation. The distillation was carried out rapidly using an oil bath to prevent local overheating as thioglycolic acid loses water to polymerize under these conditions.[3]

Standard solutions of thioglycolic acid were prepared by direct weight in air-free water. These solutions did not change titer within one week.

Analysis.—Ten to 25 ml of approximately 0.1*M* solutions prepared by weight in air-free water was introduced into 20 ml of an air-free solution of 1.0*N* sulfuric acid containing starch indicator and a slight excess of potassium iodide over the number of moles of thioglycolic acid added. This solution was then titrated to the blue iodine end point with air-free 0.10*N* potassium iodate, a stream of nitrogen being passed over the solution during the titration.

Iodine, which is liberated upon the addition of iodate, oxidizes thioglycolic acid to dithiodiglycolic acid, $HOOCCH_2SSCH_2CO_2H$ (7). In the presence of air, a slight induced oxidation of the thioglycolic acid occurs.

Preparation of dithiodiglycolic acid.—Dithiodiglycolic acid was prepared from pure thioglycolic acid by oxidation with ferric alum in 0.1*N* sulfuric acid. The ferric solution was slowly added to the thioglycolic acid in 0.1*N* sulfuric acid until spot tests with potassium thiocyanate indicated an excess of ferric iron in the solution. The oxidized solution was extracted with ether, the ether layer separated, and evaporated to dryness. The white crystals remaining were twice recrystallized from ethyl alcohol.

Polarography of thioglycolic acid.—A Sargent Model XII photographic and a manual polarograph were used in the present work. The manual polarograph was of the type described by Kolthoff and

[1] Manuscript received December 11, 1952. This paper was prepared for delivery before the New York Meeting, April 12 to 16, 1953.

[2] The experimental part of the present work was reported to the U. S. Public Health Service in November 1950.

[3] The distilled thioglycolic acid was stored at 0°C and the bottle in which it was kept was flushed with nitrogen during and after the removal of samples. Using this procedure, the extent of oxidation was less than 1 per cent in one and a half years. Thiolactides slowly formed, however, at the rate of about 0.5 per cent for each 3 months of storage.

Lingane (8) with a galvanometer having a 10-second period. All measurements were made at 25 ± 0.1°C with an external saturated calomel electrode, SCE. Two capillaries were used: capillary I—m = 1.366 mg/sec and t = 4.53 sec in 0.10N KCl with a closed circuit at a height of mercury of 80 cm; capillary II—m = 1.005 mg/sec and t = 5.92 sec with a closed circuit and a height of 70 cm.

All experiments were carried out at 25.0 ± 0.1°C.

Results and Discussion

Polarograms were obtained for $10^{-3}M$ solutions of thioglycolic acid in buffers with *pa*H between 1.0 and 12.45. In all of these solutions an anodic wave was observed (see Fig. 1). Throughout the *p*H range investigated, this wave is well shaped and clearly defined with no evidence of maxima or irregularities observed by Kolthoff and Barnum (2) for the anodic wave of cysteine. The height of the thioglycolic acid wave was found to be proportional to the concentration at least up to 3 × $10^{-3}M$. The half wave potential was found to be independent of the concentration of the thioglycolate ion within the experimental error.

No specific buffer effect was observed in these solutions as sometimes occurs in the polarography of organic compounds. In regions where buffers overlap, the half wave potential is a function of only the *pa*H (negative logarithm of the hydrogen-ion activity) and not of the buffer anions.

A small prewave appears at values of *pa*H less than 4.6. This becomes more prominent as the *pa*H decreases. This wave is not well developed and its height is difficult to measure. In 0.1M perchloric acid, 0.1M sodium perchlorate, its height appears to decrease slightly with increase in the concentration of thioglycolic acid. In several respects the prewave has the characteristics of an adsorption current (9).

A second anodic wave at more positive potentials than the wave described above is observed in acid buffers where the dropping electrode can be made sufficiently positive vs. SCE before the dissolution of mercury [see also (1)]. This second anodic wave is steep and on the limiting current region the galvanometer oscillations are erratic. In a solution of *p*H 1.0 this wave appears at about 0.23 volt vs. SCE. At this *p*H the height of the second wave (over the first wave) does not increase with the concentration of thioglycolic acid in solutions over $10^{-3}M$ while the height of the total first wave (prewave plus normal wave) is proportional to the concentration.

Stricks and Kolthoff (3) in the polarography of glutathione found two anodic waves similar in shape and behavior to those found for thioglycolic acid. They attribute the second wave to the formation of a Hg(II) compound of the type

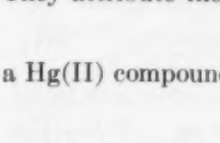

Diffusion coefficients were calculated for the species, $HSCH_2CO_2H$, $HSCH_2CO_2^-$, and $^-SCH_2CO_2^-$ by means of the Ilkovic equation (10),

$$i_d = 607nD^{1/2}Cm^{2/3}t^{1/6}.$$

Assuming (v.i.) that n, the number of electrons involved in the oxidation per molecule of thioglycolate, is equal to one for the first anodic wave, the diffusion coefficients were calculated to be 9.2, 11.3, and 9.7 × 10^{-6} cm²/sec for RSH_2, RSH^-, and $RS^=$, respectively, at 25°C.

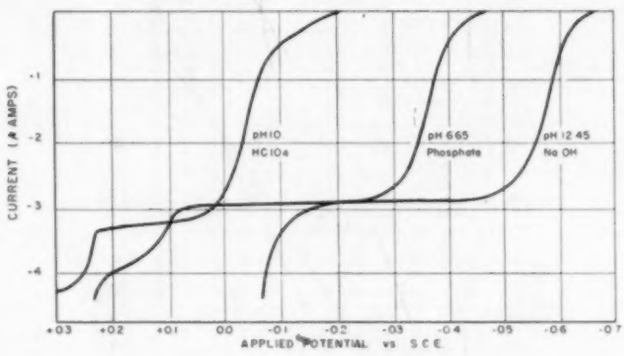

Fig. 1. Current-voltage curve of 1.10 × $10^{-3}M$ thioglycolic acid in various buffers (not corrected for residual current).

Elving and Tang (11) report values of the diffusion coefficients of undissociated chloroacetic acids to be 10.0 × 10^{-6} cm²/sec and Kolthoff and Barnum (2) report a value for cysteine to be 7 × 10^{-6} cm²/sec. Thus, it may be safely concluded that the anodic wave of thioglycolic acid involves one electron.

Liberti and Cervone (1) report values from which the diffusion coefficient of thioglycolic acid is calculated to be 8.6 × 10^{-6}, but they do not mention any effect of *p*H.

Analysis of the Wave

The current-voltage curve of the first anodic wave of the monobasic thioglycolate ion in a buffer of 0.05M Na_2HPO_4, 0.05M NaH_2PO_4 at a *pa*H of 6.65 was analyzed. A plot (Fig. 2) of the log $i_d - i/i$ vs. the applied potential, $E_{app.}$, gave a straight line, while a plot of log $(i_d - i)^2/i$ vs. $E_{app.}$ gave a curved line. During the anodic oxidation of thioglycolic acid at the dropping electrode a mercury compound is formed and not the disulfide. The primary electrode reactions may be given by equations (I) or (II).

$$HSCH_2CO_2^- \rightleftarrows \cdot SCH_2CO_2^- + H^+ + e^- \quad (I)$$
$$HSCH_2CO_2^- + Hg \rightleftarrows HgSCH_2CO_2^- + H^+ + e^- (II).$$

Both equations would give expression (III)

$$E_{app.} = E_{1/2} + 0.059 \log i/i_d - i. \quad \text{(III)}$$

In Fig. 2 a slope of 0.050 volt of line I is found instead of the theoretical value of 0.0591. The authors' system behaves similar to cysteine (2) and glutathione (3) at the dropping electrode.

On the other hand, Liberti and Cervone (1) claim that thioglycolic acid and cysteine give waves that correspond to an equation of the form

$$E_{app.} = K + \frac{0.059}{2} \log \frac{i}{(i_d - i)^2} \quad \text{(IV)}$$

They state that this behavior was observed after correcting their current-voltage curves for the *IR* drop in their polarographic circuit, but it is not clear how they calculated and applied the correction. The results shown here (corrected for *IR*) do not agree with their conclusion (see curve II, Fig. 2).

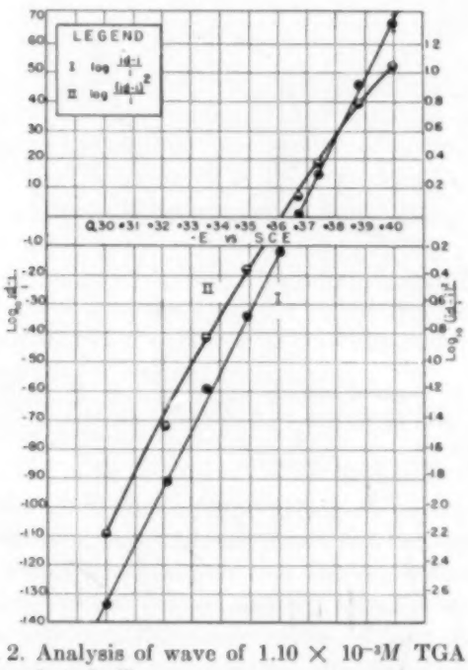

FIG. 2. Analysis of wave of $1.10 \times 10^{-3}M$ TGA in *p*H 6.65 phosphate buffer.

Moreover, measurements of the half wave potential of thioglycolate in *p*H 6.65 buffer made with the low resistance Sargent Model XII photographic polarograph gave values of -0.367 volt vs. SCE for a $6.6 \times 10^{-4}M$ solution of thioglycolate and -0.362 volt for a $3.3 \times 10^{-3}M$ solution. Assuming a total circuit resistance of 1,000 ohms, the corrected half wave potentials become -0.368 and -0.367 volt vs. SCE, respectively. Within the experimental error the half wave potential is, thus, seen to be independent of the concentration. This behavior is in accordance with equation (III). If equation (IV) were obeyed, a shift of about 20 millivolts in the half wave potential should have been observed for a five-fold change in thioglycolate.

Considering the variation of the half wave potential with *p*H, let RSH_2, RSH^- and $RS^=$ refer to the species formed in the various steps of ionization of thioglycolic acid.

The potential of the electrode at which reversible reaction (II) takes place is

$$E - E^0 + 0.059 \log \frac{a^0_{HgRS} - a^0_{H^+}}{a^0_{RSH^-}} \quad \text{(V)}$$

in which a^0 represents the activity at the electrode surface of the species denoted by the subscript. This equation can be written in terms of concentrations

$$E = E^0 + 0.059 \log a_{H^+} + 0.059 \log \frac{[HgRS^-]^0}{[RSH^-]^0} \quad \text{(VI)}$$

assuming the activity coefficients of both univalent ions equal.

Except for slight changes in the diffusion coefficients, the height of the anodic wave is independent of the stage of ionization of thioglycolic acid. The diffusion current, i_d, of this wave is given by the equation:

$$i_d = k([RSH_2] + [RSH^-] + [RS^=]) \quad \text{(VII)}$$

where the quantities in the brackets refer to the concentrations in the bulk of the solution and k is equal to $607\, nD^{1/6}m^{2/3}t^{1/6}$. D will be set equal to a mean value for all species of thioglycolic acid. This approximation is a minor one.

At any point on the current-voltage curve the current, i, is proportional to the difference of the concentrations of the diffusing species in the bulk of the solution and at the electrode surface, hence, the sum of the concentrations at the electrode surface

$$[RSH_2]^0 + [RSH^-]^0 + [RS^=]^0 = \frac{i_d - i}{k}. \quad \text{(VIII)}$$

From the ionization constants of thioglycolic acid, K_1 and K_2, it can be shown that

$$[RSH^-]^0 = \frac{i_d - i}{k} \cdot \frac{1}{\frac{a_{H^+}}{K_1} \cdot \frac{\gamma_1}{\gamma_0} + 1 + \frac{K_2}{a_{H^+}} \cdot \frac{\gamma_1}{\gamma_2}} \quad \text{(IX)}$$

where γ_0, γ_1, and γ_2 refer to the activity coefficients of uncharged, univalent, and divalent species.

The concentration of the oxidation product, $HgRS^-$, at the electrode surface can also be expressed in terms of the current, i, by the equation:

$$[HgRS^-]^0 = \frac{i}{k'}. \quad \text{(X)}$$

Substituting equations (IX) and (X) into (VI) yields

$$E_{app.} = E^0 + 0.059 \log \frac{k}{k'} + 0.059 \log \left(\frac{a_{H^+}^2}{K_1} \cdot \frac{\gamma_1}{\gamma_0} + a_{H^+} + K_2 \frac{\gamma_1}{\gamma_2} \right) + 0.059 \log \frac{i}{i_d - i}. \quad \text{(XI)}$$

The ratio k/k' is equal to the square root of the ratios of the diffusion coefficients of the reduced to oxidized forms and is about equal to one.

TABLE I. *Half wave potential of $10^{-3}M$ thioglycolic acid solutions as a function of paH at ionic strength of 0.2 capillary I, h_{Hg} = 80 cm*

paH	Buffer	$E_{1/2}$ (obs.) vs. SCE	$E_{1/2}$ calc.
12.45	0.01M NaOH	−0.58	—
10.4	0.2M NH_4Cl, 1.0M NH_4OH	−0.56	−0.565
10.1	0.2M NH_4Cl, 0.5M NH_4OH	−0.55	−0.557
10.1	0.05M $NaHCO_3$, 0.05M Na_2CO_3	−0.55	−0.557
9.5	0.2M NH_4Cl, 0.1M NH_4OH	−0.52	−0.530
9.1	0.2M NH_4Cl, 0.05M NH_4OH	−0.50	−0.510
8.7	0.2M NH_4Cl, 0.02M NH_4OH	−0.47	−0.487
7.78	0.005M NaH_2PO_4, 0.05M Na_2HPO_4	−0.43	−0.434
6.75	0.05M NaH_2PO_4, 0.05M Na_2HPO_4	−0.38	−0.373
5.75	0.05M NaH_2PO_4, 0.005M Na_2HPO_4	−0.31	−0.313
5.62	0.20M NaOAc, 0.02M HOAc	−0.31	−0.306
4.60	0.20M NaOAc, 0.20M HOAc	−0.26	−0.245
(3.55	0.20M NaOAc, 2.0M HOAc	−0.20	−0.169)
(1.0	0.10M $HClO_4$, 0.10M $NaClO_4$	−0.044	+0.112)

The half wave potential, $E_{1/2}$, is then given by the equation:

$$E_{1/2} = E^0 + 0.059 \log \left(\frac{a_{H^+}^2}{K_1} \cdot \frac{\gamma_1}{\gamma_0} + a_{H^+} + K_2 \cdot \frac{\gamma_1}{\gamma_2} \right).$$

The values of $E_{1/2}$ observed as a function of pH are given in Table I and Fig. 3. The ionic strength of all the solutions was 0.2. Using values of $\gamma_0 = 1$, $\gamma_1 = 0.76$, and $\gamma_2 = 0.38$ as given by Kielland (6), and values of K_1 equal to 2.5×10^{-4} and K_2 equal to 2.8×10^{-11}, a value of E^0 equal to +0.025 volt vs. SCE was calculated from the observed $E_{1/2}$ at a paH of 12.45. Values of $E_{1/2}$ were then calculated at other measured values of paH and are also given in Table I.

The agreement of the observed values of $E_{1/2}$ with those calculated is good. At values of paH of 4.60 and less, a deviation of the calculated values to more positive potentials than those observed is noticed. The prewave also appears in this region of paH.

Polarography of Dithiodiglycolic Acid

Fig. 4 gives polarograms obtained for $1.02 \times 10^{-3}M$ solutions of dithiodiglycolic acid in buffers of pH 3.00, 4.58, and 8.73. The cathodic waves were irregular and drawn out indicating irreversible electrode processes. The wave obtained in a phosphate buffer at pH 3.0 exhibits a flat maximum that extends over a range of about 0.6 volt. The maximum

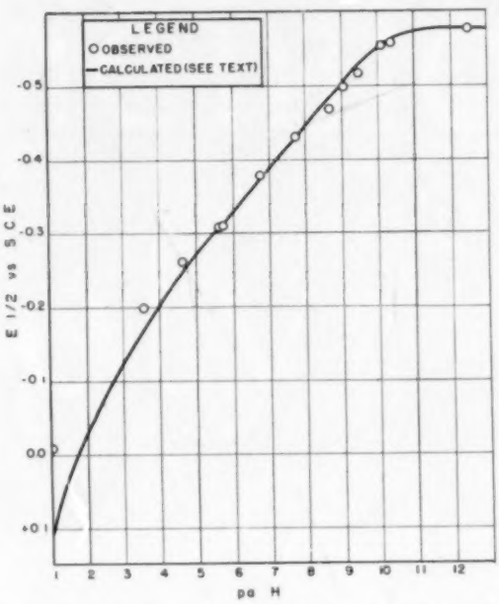

FIG. 3. Half wave potential of thioglycolic acid as a function of paH.

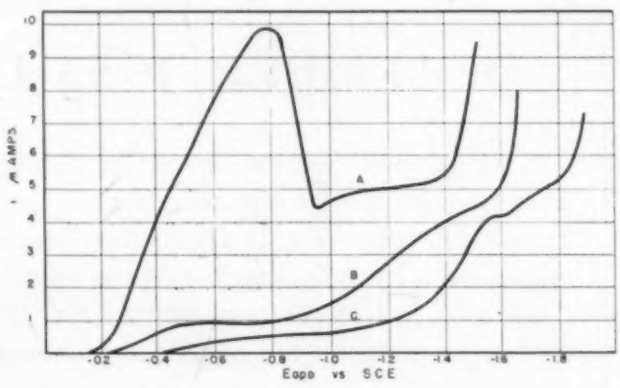

FIG. 4. Reduction of 1.02×10^{-3} M dithiodiglycolic acid. Capillary I, ht = 80 cm; A—phosphate buffer, pH 3.00; B—acetate buffer, pH 4.58; C—ammonia buffer, pH 8.73.

can be suppressed by 0.002 per cent gelatin, but in the range −0.25 to −0.95 volt vs. SCE the galvanometer oscillations remain erratic. The gelatin has no effect on the height of the normal diffusion current. In this buffer with 0.002 per cent gelatin the half wave potential was about −0.37 volt vs. SCE. The diffusion coefficient calculated in this solution is 6×10^{-6} cm²/sec assuming a two electron reduction. This value is close to the value of $5.3 \times$

10^{-6} cm^2/sec calculated for cysteine by Kolthoff and Barnum (2).

ACKNOWLEDGMENT

Acknowledgment is made to the U. S. Public Health Service for a grant which enabled this work to be carried out.

Any discussion of this paper will appear in a Discussion Section to be published in the June 1954 issue of the JOURNAL.

REFERENCES

1. A. LIBERTI AND E. CERVONE, *Ann. chim. Rome*, **41**, 95 (1951); see also SARTORI AND A. LIBERTI, *Proc. Intern. Polarogr. Congr. Prague*, Pt. I, 250 (1951).
2. I. M. KOLTHOFF AND C. P. BARNUM, *J. Am. Chem. Soc.*, **62**, 3061 (1940).
3. W. STRICKS AND I. M. KOLTHOFF, *J. Am. Chem. Soc.*, **74**, 4646 (1952).
4. E. LARSSON, *Z. anorg. u. allgem. Chem.*, **172**, 375 (1928).
5. D. G. BUSH, unpublished results.
6. J. KIELLAND, *J. Am. Chem. Soc.*, **59**, 1675 (1937).
7. P. CLAESSON, *Ber.*, **14**, 409 (1881); E. K. FISCHER, *J. Biol. Chem.*, **89**, 753 (1930); L. R. RYKLAN AND C. L. A. SCHMIDT, *Univ. Calif. (Berkeley) Publ. Physiol.*, **8**, 257 (1944).
8. I. M. KOLTHOFF AND J. J. LINGANE, "Polarography," 2nd. ed., p. 297, Interscience Publishers, Inc., New York (1952).
9. R. BRDICKA, *Collection Czechoslov. Chem. Communs.*, **12**, 522 (1947).
10. D. ILKOVIC, *Collection Czechoslov. Chem. Communs.*, **6**, 488 (1934).
11. P. J. ELVING AND CHING-SIANG TANG, *J. Am. Chem. Soc.*, **72**, 3244 (1950).

DECEMBER 1953 DISCUSSION SECTION

A Discussion Section, covering papers published in the January–June 1953 JOURNALS, is scheduled for publication in the December 1953 issue. Those who plan to contribute remarks for this Discussion Section should submit their comments or questions in triplicate to the managing editor of the JOURNAL, 235 West 102nd Street, New York 25, N. Y., not later than August 15, 1953. All discussions will be forwarded to the author, or authors, for reply before being printed in the JOURNAL.